A global inventory of stratospheric NO_y from ACE-FTS

A. Jones,[1] G. Qin,[1] K. Strong,[1] Kaley A. Walker,[1,2] C. A. McLinden,[3] M. Toohey,[4] T. Kerzenmacher,[5] P. F. Bernath,[2,6] and C. D. Boone[2]

Received 8 December 2010; revised 27 May 2011; accepted 8 June 2011; published 9 September 2011.

[1] The Atmospheric Chemistry Experiment Fourier Transform Spectrometer (ACE-FTS) on board the Canadian SCISAT-1 satellite (launched in August 2003) measures over 30 different atmospheric species, including six nitrogen trace gases that are needed to quantify the stratospheric NO_y budget. We combine volume mixing ratio (VMR) profiles for NO, NO_2, HNO_3, N_2O_5, $ClONO_2$, and HNO_4 to determine a zonally averaged NO_y climatology on monthly and 3 month combined means (December–February, March–May, June–August, and September–November) at 5° latitude spacing and on 33 pressure surfaces. Peak NO_y VMR concentrations (15–20 ppbv) are situated at about 3 hPa (~40 km) in the tropics, while they are typically lower at about 10 hPa (~30 km) in the midlatitudes. Mean NO_y VMRs are similar in both the northern and southern polar regions, with the exception of large enhancements periodically observed in the upper stratosphere and lower mesosphere. These are primarily due to enhancements of NO due to energetic particle precipitation and downward transport. Other features in the NO_y budget are related to descent in the polar vortex, heterogeneous chemistry, and denitrification processes. Comparison of the ACE-FTS NO_y budget is made to both the Odin and ATMOS NO_y data sets, showing in both cases a good level of agreement, such that relative differences are typically better than 20%. The NO_y climatological products are available through the ACE website and are a supplement to the paper.

Citation: Jones, A., G. Qin, K. Strong, K. A. Walker, C. A. McLinden, M. Toohey, T. Kerzenmacher, P. F. Bernath, and C. D. Boone (2011), A global inventory of stratospheric NO_y from ACE-FTS, *J. Geophys. Res.*, *116*, D17304, doi:10.1029/2010JD015465.

1. Introduction

[2] Total reactive nitrogen, known as NO_y, consists of active nitrogen, NO_x (NO and NO_2), and all oxidized nitrogen species, including NO_3, HNO_3, N_2O_5, $ClONO_2$, $BrONO_2$, and HNO_4. NO_x plays an important role in the atmosphere as it is involved in reactions involving hydrogen and halogen species, in particular the catalytic cycles that are responsible for stratospheric ozone loss (in addition to other reactions involving hydrogen, and halogen species). NO_y makes the largest contribution to ozone depletion in the middle stratosphere through the NO_x cycle [*Wennberg et al.*, 1994; *Intergovernmental Panel on Climate Change/Technology and Economic Assessment Panel* (*IPCC/TEAP*), 2005]. Thus, changes in the amount of NO_y or changes in the partitioning of total reactive nitrogen between NO_x and the other constituents will have an impact on the ozone budget [*IPCC/TEAP*, 2005; *Strong et al.*, 2005, and references therein].

[3] Increases in NO_y concentrations in the stratosphere are expected due to increasing tropospheric N_2O, which has an estimated atmospheric lifetime of 114 years [*Montzka et al.*, 2003]. The primary source for stratospheric NO_y is oxidation of N_2O transported from the troposphere in the tropics to the lower stratosphere [*McElroy and McConnell*, 1971; *Crutzen*, 1971; *Minschwaner et al.*, 1993; *Volk et al.*, 1997; *McLinden et al.*, 2003; *Morgan et al.*, 2004]. Because NO_y is formed at the expense of N_2O, an anticorrelation is to be expected between NO_y and N_2O [*Fahey et al.*, 1990]. N_2O has been rising approximately linearly at a rate of 0.26% per year for the past few decades [*Forster et al.*, 2007], mainly due to enhanced microbial production from agricultural expansion. N_2O has been reported to be the single most important ozone-depleting emission and is expected to remain so during the 21st century [*Ravishankara et al.*, 2009]. The World Meteorological Organization suggested that observed N_2O increases and ozone decreases explained a trend in the NO_2 total column of 5 ± 1% per decade [*World Meteorological Organization* (*WMO*), 2003]. Additionally, the WMO estimated a linear increase of NO_2 of 6.2 ± 1.8% per decade (AM) and 5.7 ± 1.1% per decade (PM) at Lauder, New Zealand (45°S) using UV-visible absorption spectroscopy from late 1980 to early 2006 [*WMO*, 2007], which is not significantly

[1]Department of Physics, University of Toronto, Toronto, Ontario, Canada.
[2]Department of Chemistry, University of Waterloo, Waterloo, Ontario, Canada.
[3]Environment Canada, Toronto, Ontario, Canada.
[4]Leibniz Institute of Marine Sciences at University of Kiel (IFM-GEOMAR), Kiel, Germany.
[5]Belgian Institute for Space Aeronomy, Brussels, Belgium.
[6]Department of Chemistry, University of York, Heslington, York, UK.

0148-0227/11/2010JD015465

different from the 5% per decade (significant to two sigma) reported by *Liley et al.* [2000]. A linear trend of 1.5 ± 1.0% per decade has been found using measurements starting in 1985 of NO_2 total columns at Jungfraujoch (47°N) and applying the same algorithm used at Lauder [*WMO*, 2007]. The Stratospheric Aerosol and Gas Experiment (SAGE) II measurements of NO_2 also show a large hemispheric asymmetry [*Cunnold et al.*, 1991]. The available measurements have suggested that the trend of NO_2 in the southern hemisphere is significantly larger than that of the northern hemisphere [*WMO*, 2007]. This apparent hemispheric difference remains unexplained at the time of writing.

[4] The primary loss mechanism for NO_y in the upper stratosphere and lower mesosphere is the destruction of NO through the reactions [*Jackman et al.*, 2005b]

$$NO + h\nu \rightarrow N + O, \quad (1)$$

$$N + NO \rightarrow N_2 + O. \quad (2)$$

[5] The loss of stratospheric NO_y occurs via transport into the troposphere and through reactions (1) and (2). The photolysis of NO only occurs above 40 km and can be very fast in the summer upper mesosphere, but significantly slower during other seasons or at lower latitudes. The photochemical life time of NO is months at the stratopause, while decades in the lower stratosphere [*Nevison et al.*, 1997], both of which are longer than or comparable to the typical transport time scales in the lower stratosphere. NO_y is dominated by transport processes in the lower stratosphere, and photochemical reactions are enhanced with increasing altitude. In the upper stratosphere, photochemical reactions control NO_y abundances [*Nevison et al.*, 1997].

[6] A decrease in the concentration of NO_y may result from lower temperatures in the lower polar stratosphere during winter, which can lead to the formation of solid HNO_3 in or on polar stratospheric clouds (PSCs) as well as sedimentation of larger particles [e.g., *McLinden et al.*, 2001]. This results in the removal of NO_y through heterogeneous chemistry; a process named denitrification. Enhancements of NO_y have been observed because of renitrification whereby the particles evaporate at lower altitudes [*Kleinböhl et al.*, 2005; *Dibb et al.*, 2006]. Additionally, stratospheric NO_y concentrations may be disturbed by aircraft [*Thompson et al.*, 1996; *Schumann*, 1997; *Schumann et al.*, 2001; *Grewe et al.*, 2002a, 2002b]. The study of the impact of NO_x emissions by *Lee et al.* [1997] during the early 1990s showed that approximately 2% of total NO_x emissions are from aircraft. Recent simulations from 3-D chemical transport models including both civil and military aircraft emissions, yield increases of zonal mean NO_y between 156 pptv (August) and 322 pptv (May) in the northern hemisphere tropopause region [*Gauss et al.*, 2006].

[7] The partitioning of NO_y depends on latitude, season, and time of day. Figure 1 shows profiles of average NO_y and the main contributing trace gas profiles in six different latitude bands: 60°N–90°N, 30°N–60°N, 30°N–30°S, 30°S–60°S, 60°S–90°S, and 90°S–90°N, using a photochemical box model [*McLinden et al.*, 2000; *Brohede et al.*, 2008] during AM and PM both at a solar zenith angle of 90 degrees. NO is the dominant NO_y species at typically 35 km and above, while peak values of NO_2 and N_2O_5 (during AM) are at a maximum and of similar magnitude between ~30–35 km. NO_x is dominant at higher altitudes in part due to the increase in the rate of photolytic conversion of HNO_3 to NO_x with increasing altitude. Hence, HNO_3 is the dominant reactive nitrogen component below 30 km. Although N_2O_5, HNO_4, and $ClONO_2$ have relatively small mixing ratios in the lower stratosphere, they play a very important role in ozone depletion.

[8] Another source of stratospheric NO_y is from energetic particle (proton and electron) precipitation. These particles penetrate into the Earth's middle atmosphere in the polar regions, where they produce NO_x by dissociation of molecular nitrogen [*Funke et al.*, 2005a, 2008a, 2008b; *López-Puertas et al.*, 2005a; *Randall et al.*, 2006, 2007]. Enhancement of N_2O is also reported from auroral energetic electron precipitation in the mesospheric polar night [*Semeniuk et al.*, 2008]. Ground state and excited state nitrogen atoms are produced when the energetic charged particles collide, dissociating N_2 [*Porter et al.*, 1976]. NO_y constituents, such as NO, can be produced by ground state [$N(^4S)$] nitrogen atoms through the following reaction:

$$N(^4S) + O_2 \rightarrow NO + O, \quad (3)$$

or NO can be destroyed through

$$N(^4S) + NO \rightarrow N_2 + O. \quad (4)$$

[9] However, NO_y is produced in the form of NO by excited states of atomic nitrogen, such as $N(^2D)$, through [*Rusch et al.*, 1981; *Rees*, 1989; *Jackman et al.*, 2005a]

$$N(^2D) + O_2 \rightarrow NO + O, \quad (5)$$

which competes with the quenching reaction [*Vitt et al.*, 2000]

$$N(^2D) + O \rightarrow N(^4S) + O. \quad (6)$$

[10] According to *Vitt et al.* [2000], this source represents about 1–2.5% of the total stratospheric NO_y. A modeling study by *Rozanov et al.* [2005] produced an increase of reactive nitrogen by about 2 ppbv in the middle stratosphere over tropical and middle latitudes when energetic particle precipitation was included, while in the upper stratosphere over polar regions the simulated NO_y enhancement reached ~10 ppbv. The large solar storms in October/November in 2003 caused very large proton fluxes which generated substantial amounts of NO_x [*López-Puertas et al.*, 2005a], while other NO_y constituents including HNO_3 [*Orsolini et al.*, 2005; *López-Puertas et al.*, 2005b] and N_2O_5 and $ClONO_2$ [*López-Puertas et al.*, 2005b] were enhanced at the same time. *Funke et al.* [2005a] found that downward transport of upper atmospheric NO_x into the polar stratosphere explains ~9% of the NO_y source in the southern hemisphere polar vortex during May to August in 2003 (measured by the Michelson Interferometer for Passive Atmospheric Sounding (MIPAS)). More recent research by

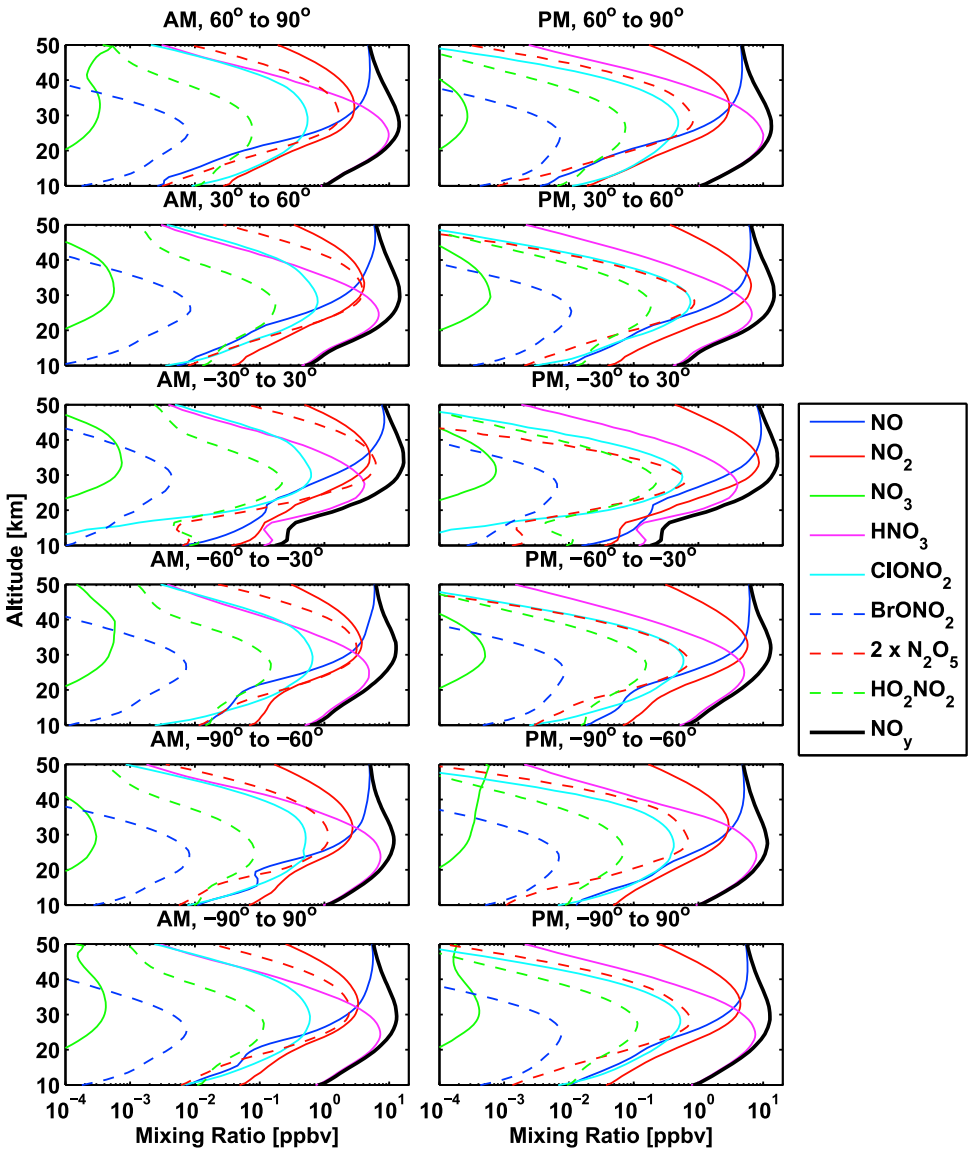

Figure 1. Modeled NO_y and individual contributing species average profiles during AM and PM time for six different latitude bands: 60°N–90°N, 30°N–60°N, 30°N–30°S, 30°S–60°S, 60°S–90°S, and 90°S–90°N. Data synthesized by a photochemical box model (see text). The results shown here use simulations made at the time and location of each ACE occultation between 2004 and 2009 with one simulation for each occultation.

Randall et al. [2007] shows that the largest energetic particle precipitation indirect effect (enhancement of NO_x in the stratosphere by descent of NO_x from the thermosphere) occurred in 1994 and 2003, contributing up to ~10% of the northern hemispheric NO_y. *Reddmann et al.* [2010] found similar enhancements in a recent modeling study.

[11] There are many models used to simulate NO_y abundances in the stratosphere [e.g., *Brasseur and Remsberg*, 1999; *Brühl et al.*, 2007]. However, evaluation of these models is difficult due to the lack of global long-term NO_y observations. In order to address this problem, we here construct a global stratospheric NO_y climatology using simultaneous measurements of major NO_y species made by the Atmospheric Chemistry Experiment (ACE), providing a new data set that can be used to test and assess atmospheric models. As ACE uses solar occultation, this data set is based on measurements made during sunrise and sunset.

2. Previous NO_y Measurements

[12] Estimation of global stratospheric NO_y concentrations requires simultaneous spaceborne measurements of the six major NO_y constituents: NO, NO_2, HNO_3, HNO_4, N_2O_5, $ClONO_2$. These "big six" account for typically 96–99% of NO_y throughout much of the lower stratosphere, while nearer to 100% above 40 km (as we will not be accounting for all NO_y species, we will use NO_y^* as the notation for the NO_y climatology). This can be seen by examining Figure 2, where NO_y^* AM and PM fractions for six different latitude bands (60°N–90°N, 30°N–60°N, 30°N–30°S, 30°S–60°S,

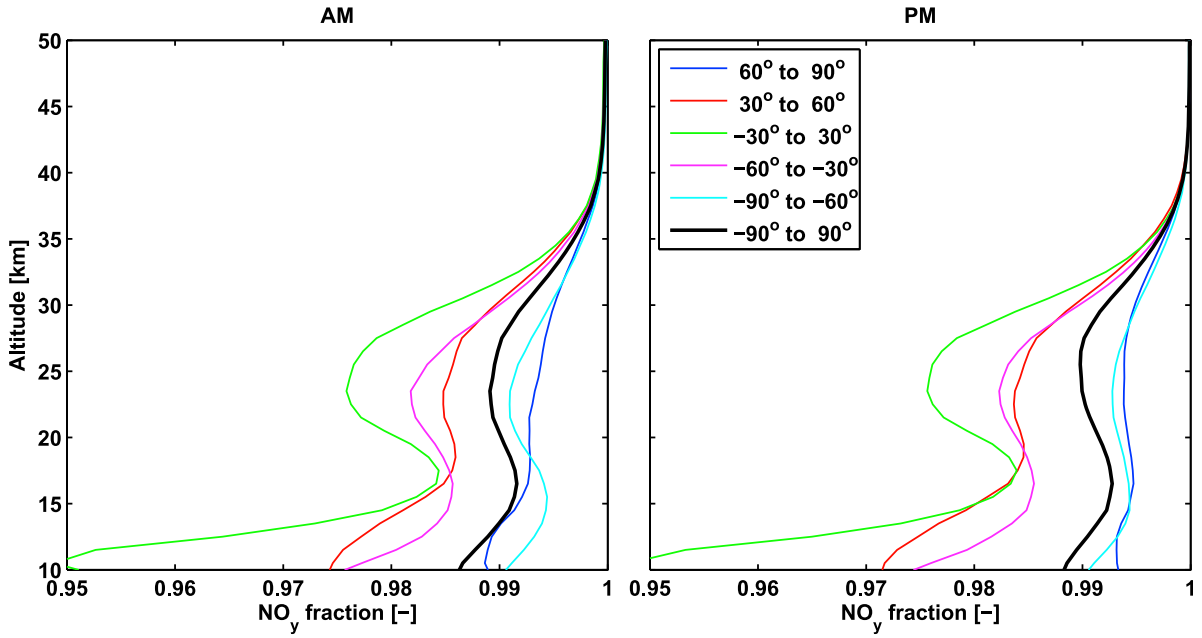

Figure 2. NO_y^* VMR fraction as a function of altitude for the six latitude bands; 60°N–90°N (blue), 30°N–60°N (red), 30°S–30°N (green), 30°S–60°S (cyan), 60°S–90°S (pink), and 90°S–90°N (black). Here, NO_y^* comprises the six main nitrogen species: NO, NO_2, N_2O_5, $ClONO_2$, HNO_3, and HNO_4.

60°S–90°S, and 90°S–90°N) have been synthesized by combining the main six species, using the same photochemical box model that produced the results in Figure 1.

[13] However, most satellite instruments measure only a few of the required species, which in some cases have been used to derive NO_y estimates. Table 1 provides a summary of all spaceborne measurements of NO_y species. The first estimates of NO_y species were made by *Gille and Russell* [1984] using nighttime measurements of LIMS HNO_3 and NO_2 (see Table 1 for definition of all instrument and satellite acronyms). The ATMOS instrument, flown on four space shuttle missions (first on Spacelab-3 in 1985 and subsequently on ATLAS 1, 2, and 3 in 1992, 1993, and 1994) was the first instrument to measure all major NO_y species (NO, NO_2, HNO_3, N_2O_5, $ClONO_2$, and HNO_4) from space [*Russell et al.*, 1988; *Abrams et al.*, 1996; *Gunson et al.*, 1996; *Zander et al.*, 1986; *Rinsland et al.*, 1994, 1985, 1996; *Zander et al.*, 1996].

[14] Five of the main six NO_y species (all apart from HNO_4) were also observed by CLAES on UARS between October 1991 and May 1993 [*Roche et al.*, 1993; *Mergenthaler et al.*, 1996; *Kumer et al.*, 1996a, 1996b], although NO retrievals were only available during the daytime. Although CLAES could make global measurements, there were limitations in that N_2O_5 retrievals below 3.16 hPa suffered from aerosol contamination, while also suffering from a lack of signal to noise and possible instrument effect above 1.47 hPa. Thus, only data for three pressure surfaces are recommended for use [*Kumer et al.*, 1996b]. A UARS pseudo-NO_y climatology was created by combining NO and NO_2 measurements from HALOE with HNO_3 and $ClONO_2$ measurements from CLAES [*Danilin et al.*, 1999], although data are perturbed by the Mount Pinatubo eruption in 1991.

[15] MIPAS on Envisat was the first instrument to measure all six major NO_y species [*Brühl et al.*, 2007; *Fischer et al.*, 2008; *von Clarmann et al.*, 2009] as well as $BrONO_2$ [*Höpfner et al.*, 2007] and it continues to operate. NO_y from MIPAS during the southern hemisphere polar vortex split in September/October 2002, was used for the study of an NO_y deficit and partitioning [*Mengistu Tsidu et al.*, 2005]. NO_x is retrieved from MIPAS using a non-LTE (Local Thermodynamic Equilibrium) algorithm [*Funke et al.*, 2005b].

[16] Recently, a stratospheric proxy NO_y climatology was constructed by combining five years of Odin observations of NO_2 from OSIRIS and HNO_3 from SMR with the photochemical box model used in Figure 1 [*Brohede et al.*, 2008]. Several merging techniques were used to derive the NO_y proxy climatology. The most appropriate merging technique used OSIRIS NO_2 to estimate NO and a weighted average of SMR HNO_3 and OSIRIS NO_2 to estimate N_2O_5 and $ClONO_2$. This survey makes apparent the lack of a global atmospheric NO_y climatology based on simultaneous measurements of all major NO_y species. This motivates the current study, which provides a more complete and up-to-date version of a NO_y climatology to help better understand the stratospheric nitrogen budget.

[17] The Atmospheric Chemistry Experiment (ACE) is built on the heritage of a number of previous solar occultation missions, particularly ATMOS. In addition, SAGE I [*McCormick et al.*, 1979], SAGE II [*Mauldin et al.*, 1985], SAGE III [*SAGE ATBD Team*, 2002], POAM II [*Glaccum et al.*, 1996] and POAM III [*Lucke et al.*, 1999; *Randall et al.*, 2002], all used UV-visible solar occultation to measure NO_2. ILAS I and II used infrared solar occultation to measure NO_2, HNO_3, $ClONO_2$, and N_2O_5 [*Sasano et al.*, 1999; *Koike et al.*, 2000; *Irie et al.*, 2006; *Nakajima et al.*, 2006; *Wetzel et al.*, 2006]. With the exception of ACE-FTS, currently there are only two other occultation instruments working in orbit that measure NO_y constituents: SCIAMACHY (NO, NO_2), which uses solar occultation

Table 1. The Record of Space-Based Measurements of NO_y Species and Corresponding References[a]

Instrument (Satellite)	Viewing Geometry	Time Period	NO	NO_2	HNO_3	$ClONO_2$	N_2O_5	HNO_4	NO_y
SAMS (Nimbus-7)	Limb emission	1979–1982	1						
LIMS (Nimbus-7)	Limb emission	1978–1979	2	2	26–27				26 (only estimate HNO_3, NO_2)
SAGE I (AEM-B)	Solar occultation	1979–1981		11–13					
SME	Limb scanning	1981–1989	3	3					
SAGE II (ERBS)	Solar occultation	1984–2003		14					
ATMOS (Shuttle)	Solar occultation	1985–1994 Four flights	71	7–15, 71	7–8, 28,71	50–52,71	7–8, 71	71	71 (used NO, NO_2, HNO_3, N_2O_5, HNO_4, $ClONO_2$)
ISAMS (UARS)	Limb emission	1991–1992	4	4	4		4, 56–57		
CLAES (UARS)	Limb emission	1991–1993	5	5	25, 32	25	32		
HALOE (UARS)	Solar occultation	1991–2005	6	6					
CIRRIS 1A (Shuttle)	Limb emission	1991			29				
MLS (UARS)	Limb emission	1991–2001			33–35				
HALOE (UARS) + CLAES (UARS)	Solar occultation + limb emission	1992–1994	6	6	25	25			70 (Used NO, NO_2, HNO_3 and $ClONO_2$)
POAM II (SPOT-3)	Solar occultation	1993–1996		16–19					
CRISTA (Shuttle)	Limb scanning	1994			30–31	30–31	31		
GOME (ERS-2)	Nadir-scanning	1995–2003		59					
ILAS I (ADEOS)	Solar occultation	1996–1997		19–26	36–38	21	54–55		
POAM III (SPOT-4)	Solar occultation	1998–2005		16, 58, 68					
SMR (Odin)	Limb emission	2001 to present			40–41				
ILAS II (ADEOS II)	Solar occultation	2002–2003		22	39	22	22		
MIPAS (Envisat)	Limb emission	2002–2004 and 2005 to present	45, 72, 75, 76	45, 66, 67, 72, 75, 76	42–45, 72, 77	53, 72, 77	42, 72, 78	45, 79	42 (used NO, NO_2, HNO_3, $ClONO_2$, N_2O_5)
SAGE III (Meteor)	Solar occultation	2002–2006		15, 68					
OSIRIS + (Odin)	Limb emission + scattering	2002–2006	3	65					69 (use HNO_3, NO_2 combined with box model)
SCIAMACHY (Envisat)	Nadir, limb and solar/lunar occultation	2002 to present	23	23, 67					
GOMOS (Envisat)	Stellar occultation	2002 to present		24, 67					
ACE-FTS (SCISAT)	Solar occultation	2003 to present	73	68, 73	73	73	73	73	
OMI (Aura)	Nadir-viewing	2003–2008		61					
MLS (Aura)	Limb emission	2004 to present			46, 47, 74				
HIRDLS (Aura)	Limb scanning	2004 to present			48–49				
GOME-2 (MetOp)	Nadir-scanning	2006 to present		60					

[a]Numbers 1–79 denote the following references: 1, *Drummond et al.* [1980]; 2, *Gille et al.* [1980]; 3, *Mount et al.* [1984]; 4, *Taylor et al.* [1993]; 5, *Roche et al.* [1993]; 6, *Russell et al.* [1993]; 7, *Abrams et al.* [1996]; 8, *Gunson et al.* [1996]; 9, *Newchurch et al.* [1996]; 10, *Manney et al.* [1999]; 11, *McCormick et al.* [1979]; 12, *Chu and McCormick* [1979]; 13, *Chu and McCormick* [1986];14, *Mauldin et al.* [1985]; 15, *SAGE ATBD Team* [2002]; 16, *Glaccum et al.* [1996]; 17, *Lucke et al.* [1999]; 18, *Randall et al.* [2002]; 19, *Sasano et al.* [1999]; 20, *Irie et al.* [2002]; 21, *Nakajima et al.* [2006]; 22, *Wetzel et al.* [2006]; 23, *Bovensmann et al.* [1999]; 24, *Kyröla et al.* [2004]; 25, *Mergenthaler et al.* [1996]; 26, *Gille and Russell* [1984]; 27, *Gille et al.* [1984]; 28, *Irion et al.* [2002]; 29, *Bingham et al.* [1997]; 30, *Offermann et al.* [1999]; 31, *Riese et al.* [1999]; 32, *Kumer et al.* [1996a, 1996b]; 33, *Santee et al.* [1999]; 34, *Santee et al.* [2004]; 35, *Waters et al.* [2006]; 36, *Koike et al.* [2000]; 37, *Irie et al.* [2002]; 38, *Nakajima et al.* [2002]; 39, *Irie et al.* [2006]; 40, *Murtagh et al.* [2002]; 41, *Urban et al.* [2005]; 42, *Mengistu Tsidu et al.* [2005]; 43, *Stiller et al.* [2005]; 44, *Wang et al.* [2007a, 2007b]; 45, *Fischer et al.* [2008]; 46, *Waters et al.* [2006]; 47, *Santee et al.* [2007]; 48, *Gille et al.* [2008]; 49, *Kinnison et al.* [2008]; 50, *Zander et al.* [1986]; 51, *Rinsland et al.* [1994, 1985, 1996]; 52, *Zander et al.* [1996]; 53, *Höpfner et al.* [2007]; 54, *Yokota et al.* [2002]; 55, *Oshchepkov et al.* [2006]; 56, *Smith et al.* [1996]; 57, *Kumer et al.* [1997]; 58, *Randall et al.* [2002]; 59, *Burrows et al.* [1999]; 60, *Callies et al.* [2004]; 61, *Levelt et al.* [2006]; 62, *Llewellyn et al.* [2004]; 63, *Fischer and Oelhaf* [1996]; 64, *Llewellyn et al.* [2004]; 65, *Brohede et al.* [2007]; 66, *Wetzel et al.* [2007]; 67, *Bracher et al.* [2005]; 68, *Kar et al.* [2007]; 69, *Brohede et al.* [2008]; 70, *Danilin et al.* [1999]; 71, *Russell et al.* [1988]; 72, *Brühl et al.* [2007]; 73, *Bernath et al.* [2005]; 74, *Urban et al.* [2005]; 75, *Funke et al.* [2005b]; 76, *Funke et al.* [2005a]; 77, *von Clarmann et al.* [2009]; 78, *Mengistu Tsidu et al.* [2004]; 79, *Stiller et al.* [2007]. Abbreviations: ACE, Atmospheric Chemistry Experiment; ADEOS, Advanced Earth Observing Satellite; AEM-B, Applications Explorer Mission-B; ATMOS, Atmospheric Trace MOlecule Spectroscopy; CIRRIS 1A, CRyogenic InfraRed Radiance Instrumentation for Shuttle; CLAES, Cryogenic Limb Array Etalon Spectrometer; CRISTA, CRyogenic Infrared Spectrometers and Telescopes for the Atmosphere; ERBS, Earth Radiation Budget Satellite; HALOE, HALogen Occultation Experiment; GOME, Global Ozone Monitoring Experiment; GOMOS, Global Ozone Monitoring by the Occultation of Stars; ILAS, Improved Limb Atmospheric Spectrometer; ISAMS, Improved Stratospheric and Mesospheric Sounder; LIMS, Limb Infrared Monitor of the Stratosphere; MIPAS, Michelson Interferometer for Passive Atmospheric Sounding; MLS, Microwave Limb Sounder; OMI, Ozone Monitoring Instrument; OSIRIS, Optical Spectrograph and Infra-Red Imager System; POAM II, Polar Ozone and Aerosol Measurement II; SAGE, Stratospheric Aerosol and Gas Experiment; SME, Solar Mesosphere Explorer; SPOT, Satellite Pour l'Observation de la Terre; UARS, Upper Atmosphere Research Satellite; SAMS, Stratospheric And Mesospheric Sounder; SCIAMACHY, Scanning Imaging Absorption spectrometer for Atmospheric CartograpHY; SMR, Sub-Millimetre Radiometer.

[*Bovensmann et al.*, 1999], and GOMOS (NO_2), using a stellar occultation technique [*Kyrölä et al.*, 2004].

[18] It should be noted that NO_y measurements have also been made using ground-based and airborne instruments. These include using in situ methods for measuring total NO_y [e.g., *Bollinger et al.*, 1983; *Fahey et al.*, 1985, 1989; *Weinheimer et al.*, 1993, 1994; *Kondo et al.*, 1996; *Schlager et al.*, 1997; *Ziereis et al.*, 2000] and using remote sensing

Table 2. Microwindows and Altitude Ranges for NO_y Species Retrieved From ACE-FTS Spectra, v2.2 Plus Updates

Species	Range for Mean Profile (km)	Microwindow		
		Center (cm^{-1})	Width (cm^{-1})	Range (km)
NO	15–110	1104.93[a]	0.30	15–35
NO	15–110	1842.95	0.30	60–110
NO	15–110	1846.62	0.30	15–110
NO	15–110	1850.20	0.30	45–110
NO	15–110	1853.70	0.30	35–110
NO	15–110	1857.17	0.45	15–110
NO	15–110	1860.75	0.30	60–110
NO	15–110	1864.30	0.30	55–105
NO	15–110	1887.53	0.40	15–110
NO	15–110	1890.80	0.40	40–110
NO	15–110	1894.00	0.45	15–110
NO	15–110	1897.00	0.45	40–110
NO	15–110	1900.00	0.30	15–110
NO	15–110	1903.17	0.35	15–110
NO	15–110	1906.15	0.30	60–110
NO	15–110	1909.13	0.30	60–110
NO	15–110	1911.98	0.35	15–110
NO	15–110	1914.96	0.30	15–110
NO	15–110	1917.82	0.30	85–110
NO	15–110	1920.70	0.30	30–55
NO	15–110	1923.46	0.24	25–45
NO_2	13–58	1581.20	0.60	15–35
NO_2	13–58	1584.15	0.50	14–35
NO_2	13–58	1584.70	0.40	14–37
NO_2	13–58	1585.40	0.90	14–38
NO_2	13–58	1586.45	0.30	14–38
NO_2	13–58	1588.70	0.30	13–37
NO_2	13–58	1590.61	0.28	14–39
NO_2	13–58	1592.57	0.30	14–40
NO_2	13–58	1595.33	0.40	15–41
NO_2	13–58	1597.10	0.50	14–58
NO_2	13–58	1598.12	0.35	13–58
NO_2	13–58	1599.93	0.55	30–58
NO_2	13–58	1602.25	0.30	15–58
NO_2	13–58	1607.99	0.58	30–58
NO_2	13–58	1611.70	0.40	15–58
NO_2	13–58	1628.73	0.44	25–58
NO_2	13–58	1629.75	0.70	20–58
NO_2	13–58	1630.97	0.30	15–58
NO_2	13–58	1634.05	0.60	28–58
NO_2	13–58	1636.88	0.40	28–58
NO_2	13–58	1641.65	0.30	18–58
HNO_3	5–37	868.10	2.20	5–32
HNO_3	5–37	872.90	2.20	5–32
HNO_3	5–37	878.50	3.00	15–35
HNO_3	5–37	1691.64	0.30	12–32
HNO_3	5–37	1698.25	0.70	25–37
HNO_3	5–37	1701.70	0.30	25–37
HNO_3	5–37	1703.05	0.40	22–37
HNO_3	5–37	1705.31	0.60	20–37
HNO_3	5–37	1716.23	0.30	25–37
HNO_3	5–37	1720.15	0.35	25–35
HNO_3	5–37	1720.89	0.40	25–35
HNO_3	5–37	1728.28	0.70	10–32
N_2O_5	15–40	1225.00	30.00	15–40
N_2O_5	15–40	1225.00	30.00	15–40
$ClONO_2$	12–35	780.15	0.60	12–20
$ClONO_2$	12–35	1104.93[b]	0.30	12–35
$ClONO_2$	12–35	1202.86[c]	0.50	12–18
$ClONO_2$	12–35	1292.60	1.60	18–35
$ClONO_2$	12–35	1728.28[d]	0.50	12–18
HNO_4	12–25	802.89	2.08	12–25

techniques to derive NO_y [e.g., *Evans et al.*, 1977; *Murcray et al.*, 1987; *Webster et al.*, 1990; *Chance et al.*, 1996; *Sen et al.*, 1998]. These measurements are localized in space and time (e.g., taken from a specific location or along a given flight path during a campaign) and thus do not provide the global stratospheric and upper tropospheric coverage provided from satellites.

3. ACE-FTS Measurements of NO_y

[19] ACE, also known as the scientific satellite SCISAT-1, was launched on 12 August 2003 and carries two instruments, the Fourier transform spectrometer (ACE-FTS) [*Bernath et al.*, 2005], and the Measurement of Aerosol Extinction in the Stratosphere and Troposphere Retrieved by Occultation (ACE-MAESTRO) [*McElroy et al.*, 2007]. Both instruments record solar occultation spectra, ACE-FTS in the infrared and ACE-MAESTRO in the UV-VIS-near-infrared. The primary objective of the ACE mission is to understand the chemical and dynamical processes that are related to ozone depletion in the stratosphere and upper troposphere, particularly in the Arctic. The ACE spacecraft is in a low-Earth circular orbit at 650 km altitude, with an inclination angle of 74°, providing up to 15 sunrise and 15 sunset solar occultations per day. The ACE orbit was chosen to optimize occultation opportunities over the tropics, midlatitudes, and polar regions with an annually repeating pattern, and with a sampling frequency which is largest over the polar regions.

[20] ACE-FTS records spectra between 750 and 4400 cm^{-1} at high resolution (0.02 cm^{-1}). Vertical profiles are calculated as a function of geometric altitude and on pressure surfaces, while temperature and volume mixing ratio (VMR) are retrieved for over 30 different trace gases. A nonlinear least squares global fitting technique is used to analyze selected microwindows. Temperature and pressure are first retrieved by analyzing CO_2 lines in the spectra, then VMR profiles are determined in a similar manner by fixing the temperature and pressure. A more detailed description of the ACE-FTS retrievals is given by *Boone et al.* [2005]. Table 2 lists the microwindows used for retrievals of all ACE-FTS NO_y species and their corresponding altitude ranges. Above the retrieval range, the initial guess profile (a priori) is scaled based on the values retrieved at the two highest points [*Boone et al.*, 2005]. The initial guess values used are based on results from the ATMOS mission.

[21] ACE-FTS scans every 2 s, where the vertical resolution of the measurements is limited to typically 3–4 km, a consequence of the instrument's field-of-view, which is circular with a diameter of 1.25 mrad. The altitude coverage of the measurements extends from the cloud tops up to 150 km, depending on the observed atmospheric gas. From the retrieval grid, VMRs are interpolated onto a separate 1 km grid. ACE-FTS can measure profiles of six NO_y species: NO, NO_2, N_2O_5, HNO_3, $ClONO_2$, and HNO_4. All but the last are part of the 14 primary target species for the ACE mission, while HNO_4 is a research product. NO_3 and $BrONO_2$ are the

Notes to Table 2:

[a] Included to improve results for interferer O_3.
[b] Included to improve results for interferer O_3.
[c] Included to improve results for interferers N_2O and CH_4.
[d] Included to improve results for interferer HNO_3.

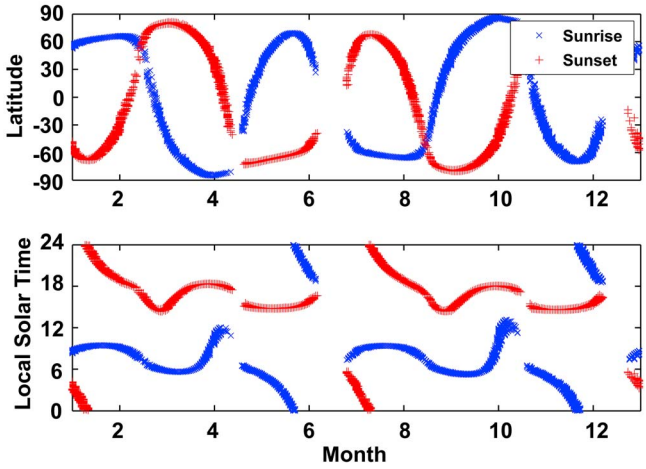

Figure 3. Locations of ACE (top) sunrise and sunset occultations and (bottom) corresponding local times.

two NO_y species not measured by ACE-FTS, but the daytime concentrations of these two species are insignificant compared to the other component species.

[22] In this work, we use ACE-FTS version 2.2 (with an update for N_2O_5), where ACE-FTS measurements of NO, NO_2, N_2O_5, HNO_3, and $ClONO_2$ and the NO_y source N_2O have been recently validated [*Kerzenmacher et al.*, 2008; *Wolff et al.*, 2008; *Strong et al.*, 2008]. ACE-FTS version 2.2 NO and NO_2 were assessed by *Kerzenmacher et al.* [2008] using space, balloon, and ground-based measurements. They concluded that the ACE-FTS NO_2 VMRs are generally consistent with other satellite data within ~20% between 20 and 40 km, with a negative bias of about −10% between 23 and 40 km. In comparison with HALOE, ACE-FTS NO VMRs agree better than ±8% from 22 to 64 km and about +10% from 93 to 105 km. ACE-FTS measurements of the reservoir gases HNO_3, $ClONO_2$, and N_2O_5 were assessed by *Wolff et al.* [2008]. The relative differences between ACE-FTS HNO_3 profiles coincident with MIPAS and MLS measurements lie within ±10% from 10 to 36 km. Overall, between 18 and 35 km, the mean relative differences of HNO_3 are better than ±20%, except for aircraft and balloon high-latitude winter comparisons, which show systematic differences to be between 20 and 30%. The relative differences between ACE-FTS and MIPAS N_2O_5 are −10% for daytime and −27% for nighttime [*Wolff et al.*, 2008]. Good agreement between ACE-FTS and MIPAS $ClONO_2$ is seen in the mean absolute differences, which are typically within ±0.01 ppbv and are not larger than −0.04 ppbv (±1%) between 16 and 27 km.

4. Methodology

4.1. Data Filtering

[23] In order to produce a NO_y^* climatology, we first construct individual climatologies for NO, NO_2, HNO_3, N_2O_5, HNO_4, and $ClONO_2$ separately. Examples of the ACE-FTS climatologies for these species (except HNO_4) have been produced and released as an official product by A. Jones et al. (A description of the ACE-FTS global climatological datasets, submitted to *Atmospheric Chemistry and Physics*, 2011). However, the climatologies considered here differ in that we include the scaled initial guess values, which are used where no actual measurement is made in a given occultation. An explanation as to why we include these values will be given later.

[24] The climatologies use a zonal average grid representing pressure as a function of latitude. We use 33 pressure surfaces, 31 of which are defined by the Chemistry Climate Model validation (CCMVal) project [*Eyring et al.*, 2010], covering ~15 to ~70 km: 1000, 850, 700, 500, 400, 300, 250, 200, 170, 150, 130, 115, 100, 90, 80, 70, 50, 30, 20, 15, 10, 7, 5, 3, 2, 1.5, 1, 0.7, 0.5, 0.3, 0.2, 0.15, 0.1 hPa (note: 0.7 and 0.15 hPa are the two pressures not defined by CCMVal). Although the pressure grid extends to 1000 hPa, one should note that there are no ACE observations made below 300 hPa. 36 latitudinal grid bins run in 5° intervals from −90°S to 90°N (e.g., the 90°S to 85°S interval is labeled as 87.5°S). In total, a grid size of 36 × 33 is produced for a given month.

[25] Observations acquired between February 2004 and February 2009 for each species are independently filtered on a monthly basis into the described grid bins. Since the profiles of NO, NO_2, and N_2O_5 exhibit strong diurnal variation, sunset and sunrise measurements should not be averaged together. Hence, further filtering is needed to separate observations such that they share similar temporal properties. This is achieved by calculating the local solar time (LST) for each occultation by using the corresponding longitude (λ, ranging from −180° to +180°) and the universal time (UT) in hours for the reference tangent point,

$$\mathrm{LST} = \mathrm{UT} + (24/360)\lambda. \tag{7}$$

[26] This equation gives LST relative to UT by adding or subtracting 24 h (to obtain values less than zero or greater than 24) to the stated UT. ACE occultations are labeled as sunrise and sunset as seen from orbit, but may not be local sunrise or sunset at the measurement location except in the tropics. This is to do with the occultation geometry of the ACE satellite. Figure 3 shows a summary of the ACE sunrise and sunset occultations and corresponding local times over 12 months. As the ACE orbit is repetitive, this plot is approximately the same annually. In this paper, we refer to measurements before local noon as local sunrise (we use AM) and after local noon as local sunset (we use PM). Ultimately, this means that we produce two separate climatologies for each species: one containing only AM observations and one containing only PM observations.

[27] While binning measurements, they are also subjected to several filtering criteria. The first is that there are various spectra that are known to have ambiguities, hence these are disregarded. These "Do Not Use" (DNU) occultations are listed and available on the ACE website: https://databace.uwaterloo.ca/validation/data_issues.php. Any observation whose fitting uncertainty that is greater than 100% of the measurement value is ignored, while any measurement with a fitting uncertainty that is smaller than 0.01% of the measurement value is also ignored. This 1-sigma fitting uncertainty is the square root of the diagonal element of the covariance matrix obtained in the retrieval process [*Boone et al.*, 2005]. In addition, negative values are not systematically removed from the data set as they can result from

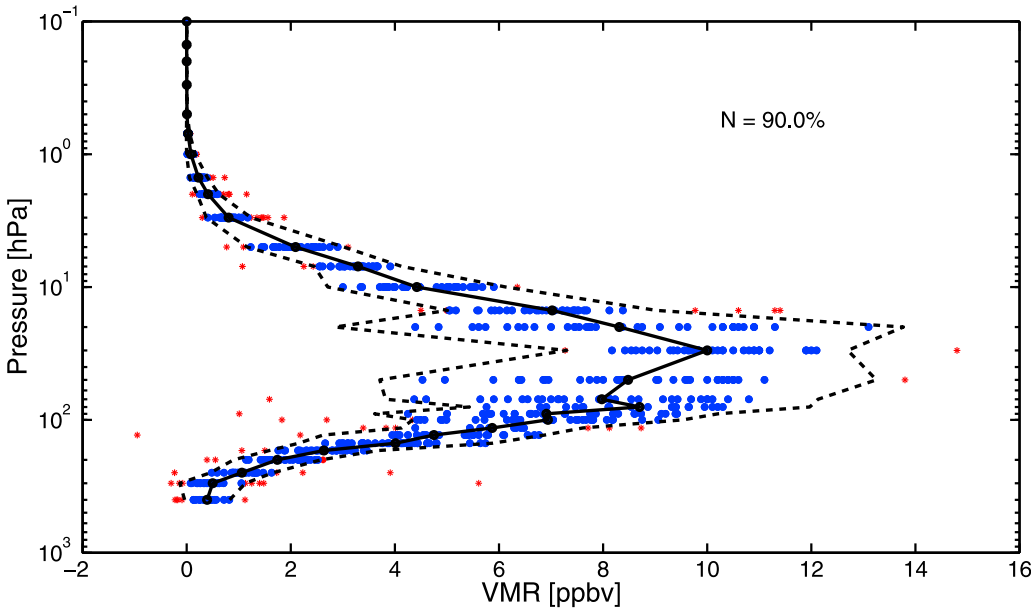

Figure 4. Example of February HNO_3 data (70°N–75°N bin, blue dots) and how outliers are removed using MAD filtering. Red stars are deemed nonrepresentative (~10%) and are thus rejected. The solid black line is the median of all observations, while the dashed line is the three-MAD envelope. N represents the percentage of retained measurements after three-MAD filtering. Here, 10% are removed.

the retrieval when there is noise in the measurements when the VMR of a particular species is low. Removing them would introduce an erroneous high bias in the data.

[28] As a climatology is the most probable state of the atmosphere for a given location and time, it is important to remove those data points which are considered nonrepresentative of the most probable state of the atmosphere for a given location. In order to do this we follow the method used by Jones et al. (submitted manuscript, 2011), who utilize the median absolute deviation (MAD), a robust statistical technique used to remove outliers from a sample

$$MAD_n = median(|x_i - M_n|). \tag{8}$$

MAD is calculated by finding the median of the absolute deviation between measurements x_i and the median, M, of a data set, size n. This method is preferred to that of a standard deviation as the MAD is less affected by extreme values. A standard deviation is dependent upon the square of the distance from the mean value; hence large deviations are heavily weighted. As can be seen from equation (8), the distance is less of an issue using the MAD when considering a small number of outliers. In order to remove nonrepresentative data, we use three MADs, which is approximately equivalent to two standard deviations (i.e., ~95% of the total population). This means that in a perfect Gaussian distribution we should expect approximately 5% of the data to be removed (deemed nonrepresentative of the average climatological state). However, due to nature not always being totally random and also due to possible biases in the measurements themselves, it is typically the case that 5–10% of data are removed. Moreover, as we also include the scaled initial guess values, it means that these nonnatural data points will force the distribution to be less Gaussian, hence the percentage of data disregarded is typically larger, 5–20%. Although this may be the case, we still find there to be a sufficient number of data remaining to produce a climatology for each species. Scaled initial guess profiles are included as they allow for full altitude coverage to be obtained. If this is not done, gaps in the individual climatological fields from each species would limit the overall information available to produce the final NO_y^* climatology.

[29] Figure 4 illustrates an example of the MAD filtering on HNO_3 PM measurements for the 70°N–75°N latitude band for February. The measurements have been filtered into the relevant pressure bins, where the blue circles in Figure 4 are the retained values after undergoing filtering using three MADs, while the red stars are considered outliers, hence not a good representation of the most probable state. To help indicate this more clearly we have drawn the median profile (Figure 4, solid black line) also accompanied by the three-MAD envelope (Figure 4, dashed lines). N indicates the percentage of retained values, which in this case is approximately 90%, implying roughly 10% of the data from this latitude bin are disregarded.

[30] The monthly filtered data that remain are used to produce a zonal average. This is done by making a quality-controlled calculation such that each measurement is weighted by the inverse of its corresponding fitting uncertainty value. Thus values with large measurement uncertainties are weighted less than those with smaller measurement uncertainties. It should also be noted that the scaled initial guess values are only considered in the mean calculation for a given bin if it contains no measurement values. This allows us to obtain a climatology with full altitude coverage and it prevents contamination of the measurements with scaled initial guess values in the weighted average calculation. For this climatology, we have decided not to set a minimum number of measurements per bin that

would otherwise determine if a zonal mean would be calculated. The ACE-FTS climatology, produced by Jones et al. (submitted manuscript, 2011), used a minimum of five values for a zonal mean to be considered hence providing a level of statistical robustness. The reason for not including this in the NO_y^* climatology is simply because by setting a grid minimum threshold potentially creates a scenario where more gaps will occur in the NO_y^* climatology grid. This is primarily due to the differences in altitude coverage between the observed gases and that the NO_y^* climatology itself is dependent on a value from each of the six nitrogen species. Instead, we have used matrices (with the same dimensions as the climatology) for each of the six nitrogen species, providing the number of measurements used to calculate the NO_y^* value for a given bin. This can be used in conjunction with the NO_y^* climatology so as to ascertain a level of confidence in each individual NO_y^* bin value.

4.2. Construction of the NO_y^* Climatology

[31] In order to produce monthly NO_y^* climatologies, we first produce AM and PM climatologies of NO_y^* by adding algebraically the individual monthly climatological fields from the contributing species, as shown in equations (9) and (10). We find that $NO^*_{y\_pm}$ and $NO^*_{y\_am}$ climatological fields show almost identical characteristics in terms of VMRs and structure. In order to produce a final NO_y^* climatological field we simply find the average of the sum of the $NO^*_{y\_am}$ and $NO^*_{y\_pm}$ fields, as given in equation (11)

$$\left[NO^*_{y\_am}\right] = [NO]_{am} + [NO_2]_{am} + [HNO_3]_{am} + 2 \times [N_2O_5]_{am} + [ClONO_2]_{am} + [HNO_4]_{am} \quad (9)$$

$$\left[NO^*_{y\_pm}\right] = [NO]_{pm} + [NO_2]_{pm} + [HNO_3]_{pm} + 2 \times [N_2O_5]_{pm} + [ClONO_2]_{pm} + [HNO_4]_{pm} \quad (10)$$

$$\left[NO^*_{y}\right] = \frac{\left(NO_{y\_am} + NO_{y\_pm}\right)}{2}, \quad (11)$$

where [ ] indicates the monthly mean of each species. In order to gain information about the magnitude of yearly variation on a monthly basis we can consider the 1 standard deviation of the data in each bin for each species. Furthermore, we can simply calculate the 1 standard deviation of a monthly NO_y^* climatology by following equations (12)–(14)

$$\sigma_{NO_{y\_am}} = \left([\sigma_{NO}]^2_{am} + [\sigma_{NO_2}]^2_{am} + [\sigma_{HNO_3}]^2_{am} + (2 \times [\sigma_{N_2O_5}])^2_{am} + [\sigma_{ClONO_2}]^2_{am} + [\sigma_{HNO_4}]^2_{am}\right)^{\frac{1}{2}} \quad (12)$$

$$\sigma_{NO_{y\_pm}} = \left([\sigma_{NO}]^2_{pm} + [\sigma_{NO_2}]^2_{pm} + [\sigma_{HNO_3}]^2_{pm} + (2 \times [\sigma_{N_2O_5}])^2_{pm} + [\sigma_{ClONO_2}]^2_{pm} + [\sigma_{HNO_4}]^2_{pm}\right)^{\frac{1}{2}} \quad (13)$$

$$\sigma_{NO_y} = \left(\frac{1}{4}\left[\sigma_{NO_{y\_am}}\right]^2 + \frac{1}{4}\left[\sigma_{NO_{y\_pm}}\right]^2\right)^{\frac{1}{2}}. \quad (14)$$

Hence, σ_{NOy_am} is determined by calculating the square root of the sum of the squares of each 1 standard deviation value calculated in each grid bin for the NO_y^* AM climatological field. Thus, we combine the 1-sigma fields from each independent species to produce a 1-sigma field for NO_y^* AM (σ_{NOy_am}) and PM (σ_{NOy_pm}). Combining these two fields using equation (14) provides a 1 standard deviation field for the NO_y^* climatology (σ_{NOy}).

4.3. Three Month NO_y^* Climatologies

[32] Combined three-monthly NO_y^* climatologies are also produced, namely, December–January–February (DJF), March–April–May (MAM), June–July–August (JJA), and September–October–November (SON). This is achieved by combining the measurements available in the monthly climatologies for each of the individual species. It should be noted that no extra MAD filtering is performed as each month is already in the best representative state. For a given 3 month period and a given nitrogen species, we take the individual prefiltered measurements from each pressure/latitude bin, which were used for the calculation of the respective individual monthly climatologies, and merge them. As an example, for the NO_2 DJF climatology, we take the individual NO_2 measurements that were used to create the climatologies for December, January, and February and merge them into the respective bins. We then use quality control, where each measurement is weighted by the inverse of its corresponding fitting uncertainty value, to produce a zonal average from the merged measurements and their respective uncertainties. This is applied to all six nitrogen species, such that six individual trace gas climatologies will be produced for a given 3 month period. In order to produce a NO_y^* three-monthly combined climatological field we then simply follow equations (9)–(11). We also make climatologies that consider AM, PM, and combined AM + PM measurements.

5. Results

5.1. Individual Species Comparison

[33] In order to illustrate the full extent of the data utilized, Figure 5 presents all postfiltered VMR profiles and scaled initial guess values for each individual NO_y^* species measured between February 2004 and February 2009, for all latitudes, all months and all times (i.e., both AM and PM local solar times). The black solid line indicates the median and the dashed line is the mean of all profiles shown. The dash-dotted lines indicate the 1 standard deviation of all the profiles. NO is plotted on a logarithmic scale because its VMR varies from 0.01 to 1000 ppbv for the full altitude range, but this also means that negative VMRs are not seen in this plot. Maximum NO VMRs are found typically between 0.1 and 1 hPa, while the break in the median and mean profile lines is due to the negative values. NO_2 has maximum VMRs of approximately 8 ppbv, typically distributed between 2 and 30 hPa. Maximum HNO_3 VMRs of about 15 ppbv are mainly distributed between 10 and 70 hPa. N_2O_5 has maximum VMRs of about 4 ppbv, distributed between 1 and 20 hPa. VMRs of $ClONO_2$ are much smaller compared to NO and NO_2, with VMRs generally less than 2.5 ppbv. Both the median and mean profiles show consis-

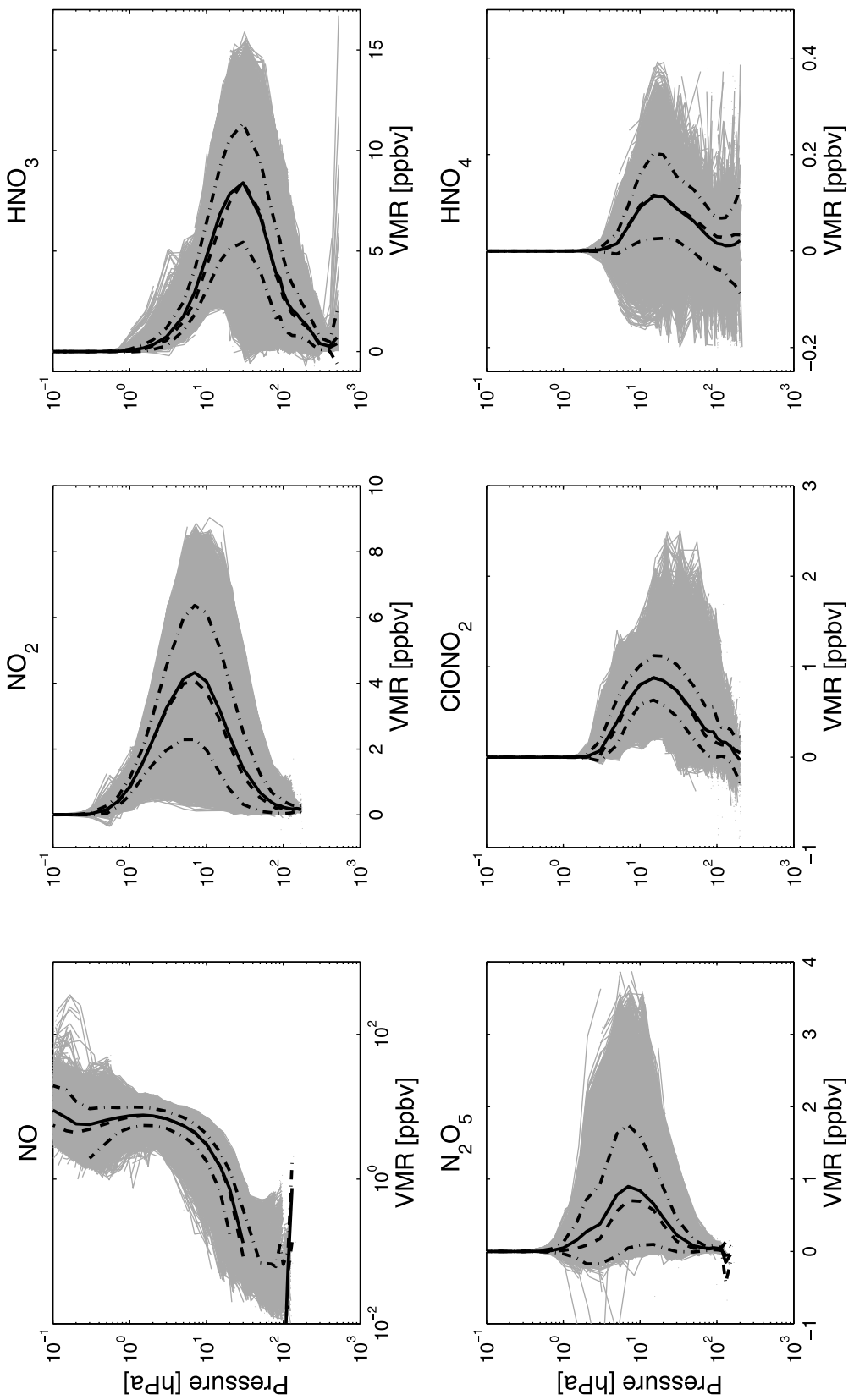

Figure 5. All ACE-FTS NO, NO_2, HNO_3, N_2O_5, $ClONO_2$, and HNO_4 profiles used in the NO_y^* climatology (shading) and the corresponding mean (black dashed lines), median profiles (solid lines), and 1 standard deviation from the mean (dash-dotted lines) from February 2004 to February 2009.

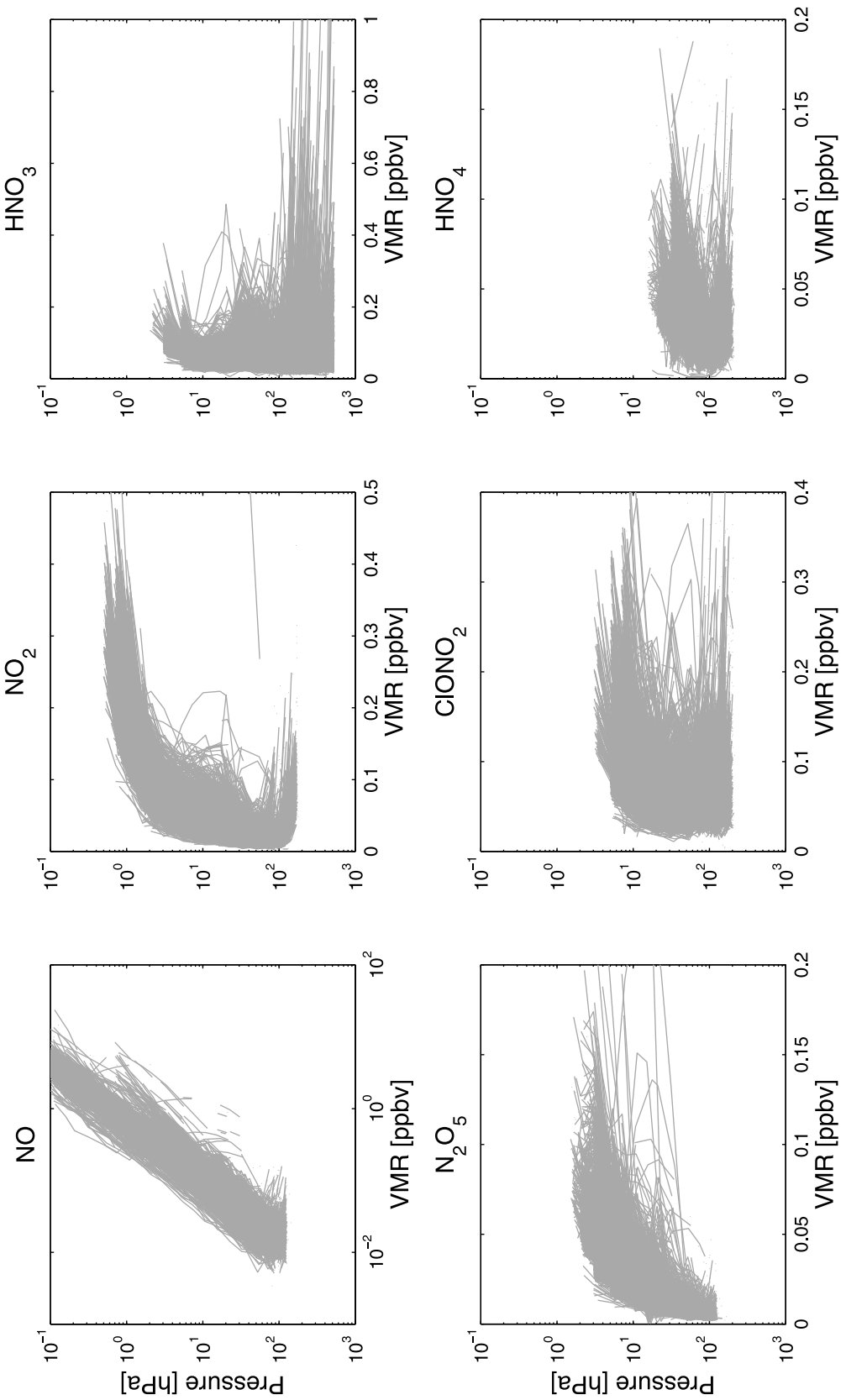

Figure 6. All ACE-FTS fitting uncertainties for NO, NO_2, HNO_3, N_2O_5, $ClONO_2$, and HNO_4 used in the climatology, from February 2004 to February 2009.

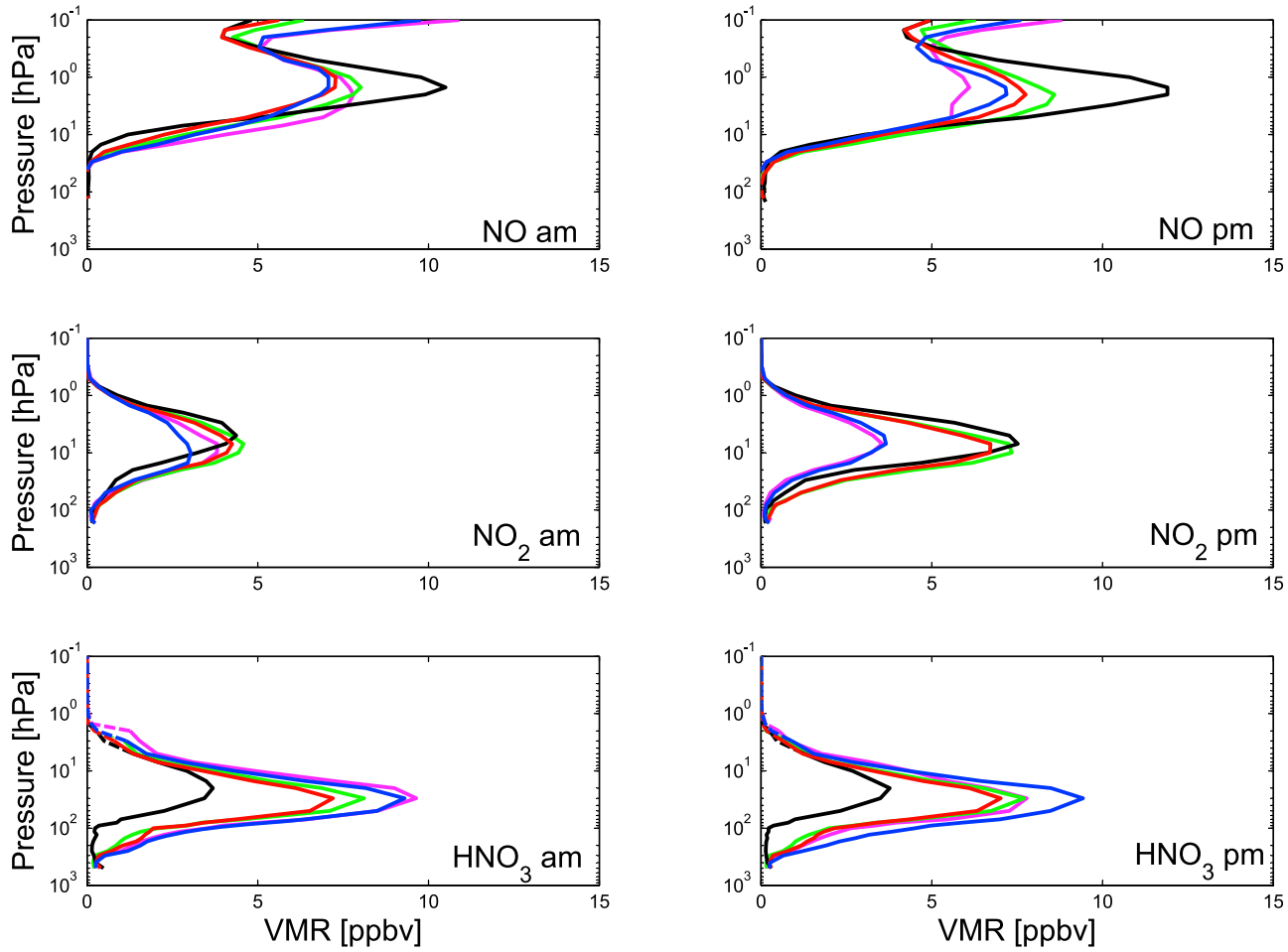

Figure 7a. Median VMR profiles of NO, NO_2, and HNO_3 in five latitude bands using ACE-FTS data from February 2004 to February 2009. (left) AM observations. (right) PM observations. Latitude bands are coded as: blue, 60°N–90°N; red, 30°N–60°N; black, 30°N–30°S; green, 30°S–60°S; pink, 60°S–90°S. Solid lines are measurements, and dashed lines are where only scaled initial guess values are considered.

tency and it can be seen that the maximum VMR is found around 20–30 hPa, of 1 ppbv. Maximum $ClONO_2$ values are typically 2.5 ppbv around this same altitude region. HNO_4 is a research product, and is difficult to measure because its VMR is so small (much less than 1 ppbv). Consequently, measured VMRs are noisy, yielding both negative and positive values throughout most of the stratosphere. However, mean and median profiles show that predominantly positive values are present with a maximum peak around 20 hPa.

[34] The fitting uncertainties corresponding to the ACE-FTS measurements from Figure 5 are shown in Figure 6. These fitting errors are for the measurements only, as all scaled initial guess values have no uncertainties given and are thus ignored in Figure 6. The fitting error is large for HNO_3 and $ClONO_2$ in the upper troposphere/lower stratosphere because concentrations of both these species are small and are thus difficult to measure. A similar scenario is seen for HNO_4, which has the largest fitting error (if one considers relative units, not shown but easily calculated) at all measurable altitudes as a result of its small VMR.

[35] Before producing the NO_y^* climatology, it is also interesting to examine the median NO_y^* VMR profiles within given latitude bands. The median AM and PM profiles of the six NO_y species in five defined latitude bands: 60°N–90°N, 30°N–60°N, 30°N–30°S, 30°S–60°S, and 60°S–90°S, are calculated from the data presented in Figure 5 and are presented in Figures 7a and 7b. It should be noted that in order to calculate these profiles, we have used the weighting quality control technique as described in section 4.1, while we also only consider scaled initial guess values at altitudes where measurements are not made. This latter point is shown in Figure 7, where the scaled initial guess values are illustrated as dashed lines, while measurements are solid lines.

[36] Significant diurnal variation is seen for NO, NO_2, and N_2O_5 as expected. It can be seen from Figure 7a that the latitudinal variation of NO VMRs is relatively small, with the equatorial median profile showing the largest difference between 1 and 10 hPa. In general, the average PM NO_2 VMRs are greater than the average AM NO_2 VMRs at all latitudes apart from the poles. For example, during PM, NO_2 VMRs in the tropics are greater than 7 ppbv, while the median AM NO_2 VMR is ~4 ppbv. The variation of NO_2 is smaller between day and night at the poles, exemplified by the average profiles for both and AM and PM NO_2 VMRs being ~4 ppbv. There is large latitudinal variation between the tropics and poles for HNO_3, with maximum VMRs of

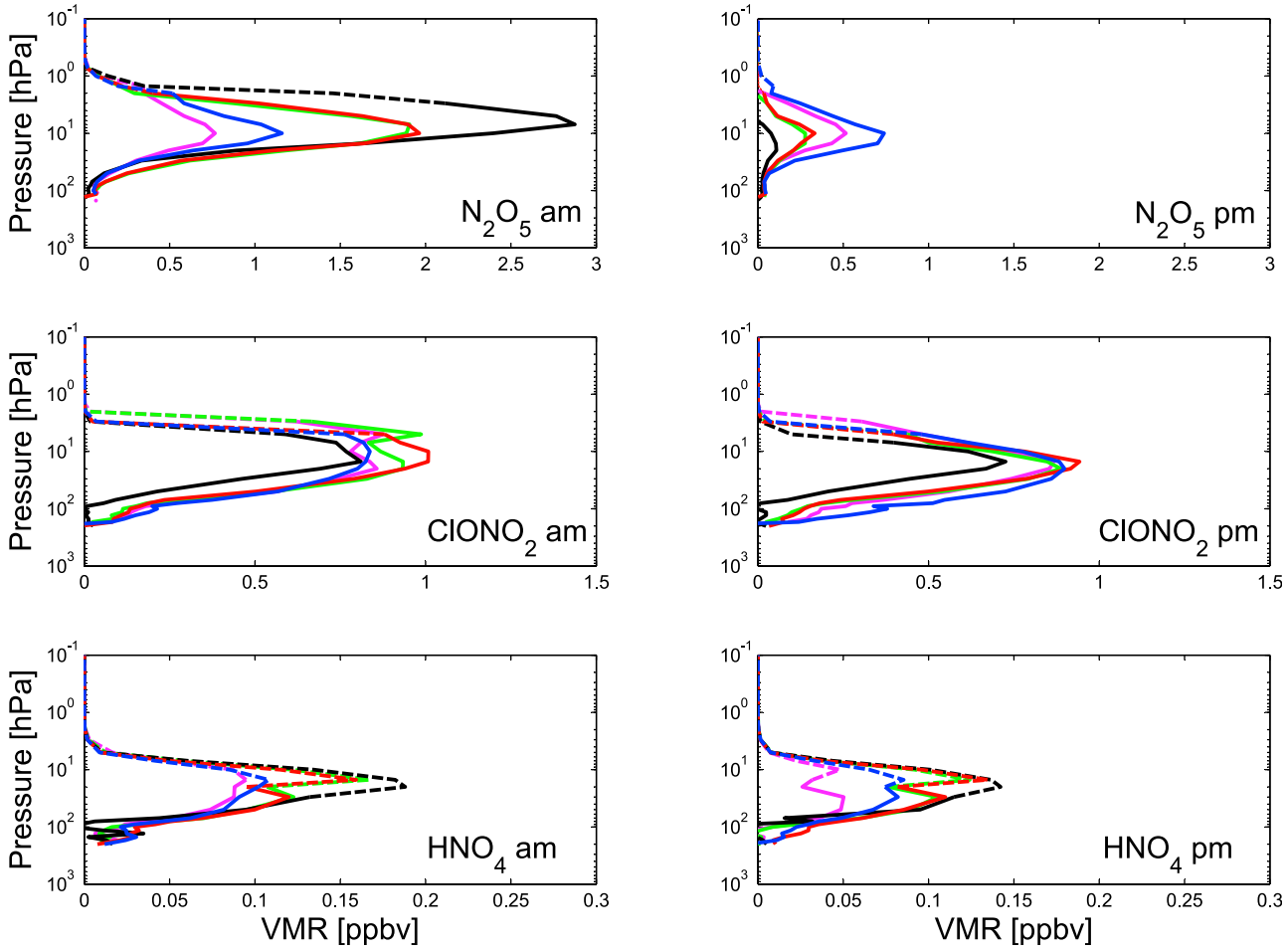

Figure 7b. Same as Figure 7a but for N_2O_5, $ClONO_2$, and HNO_4.

typically 7–9 ppbv between 20 and 50 hPa seen at polar latitudes. For N_2O_5 in Figure 7b, median AM VMRs are much larger than the median PM N_2O_5 VMRs at all latitudes, where the largest difference of about 2.1 ppbv is seen in the tropics. Peak N_2O_5 VMRs during PM are less than 1 ppbv at all latitudes. $ClONO_2$ shows little diurnal and geographical variation. Here, VMR maxima are in the vicinity of 0.7–1 ppbv, located close to 10 hPa. Diurnal and latitudinal variability for HNO_4 is moderate. The median AM VMRs are typically larger than 0.1 ppbv but less than 0.2 ppbv, while the median PM VMRs are greater than 0.05 ppbv but less than 0.15 ppbv.

[37] One feature that is apparent in both the $ClONO_2$ (AM) and HNO_4 (AM and PM) are the local minima seen for some latitude bins. While the $ClONO_2$ minima are believed to be related to the measurements themselves, we find the HNO_4 local minima to be associated with the scaled initial guess values, which have a tendency to be unrealistically large at altitudes where the measurements stop.

[38] Figure 8 illustrates the median NO_y^* profiles in the same five latitude bands by combining the individual profiles for AM and PM from Figures 7a and 7b. Visual inspection of this diurnal comparison reveals little variation between the same latitudes. The largest difference can be seen for the southern hemisphere polar bin, where AM maxima are ~1 ppbv larger than during PM maxima. This may be due to differences in the AM and PM sampling of southern polar latitudes, which are heavily influenced by a large degree of natural variability from EPP and mesospheric descent. This is illustrated by the 1 standard deviation of the NO_y^* VMR for this latitude band that shows AM to have a larger variation in the upper stratosphere compared to PM. Comparison of the latitudinal bins shows that peak tropical NO_y^* VMRs are situated typically higher in the stratosphere in comparison to the midlatitudes and polar regions, which is a result of strong vertical transport of N_2O in the tropics, where it is oxidized at these higher altitudes. A more quasi-horizontal transport is experienced in the extratropics where upwelling is weaker compared to the tropics and thus N_2O oxidation occurs lower in the stratosphere.

5.2. NO_y^* Monthly Climatologies

[39] Figure 9 illustrates the NO_y^* monthly climatological fields calculated using the method described in section 4. The quality-controlled zonally averaged data are shown, for each month in each grid bin, represented by pressure as a

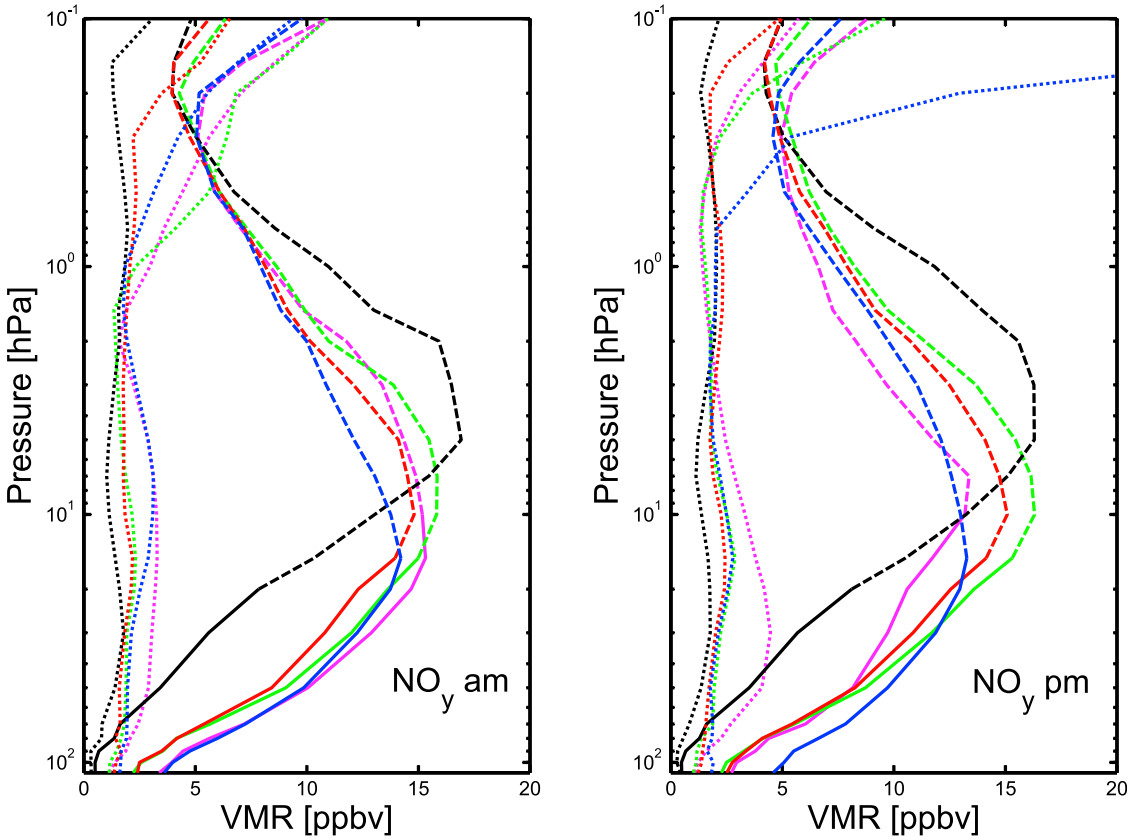

Figure 8. Same as Figure 7 but for NO_y^*. Dashed lines indicate where scaled initial guess values contribute to the median value. Dotted lines indicate the 1 standard deviation spread of data in each latitude bin.

function of five degrees latitude. Missing data are where ACE-FTS does not make a measurement.

[40] Peak NO_y^* VMRs are at higher altitudes in the tropics (typically above 10 hPa) compared to the midlatitudes and poles (typically 10 to 80 hPa). In the tropics, maximum VMRs of NO_y^* are generally between 16 and 20 ppbv. It can also be seen that the polar winter/spring contains less NO_y^*. This asymmetry is because the polar vortex, which forms during the winter, is diluted with NO_y-depleted air that descends from the upper stratosphere due to the Brewer-Dobson circulation. There is also strong evidence during August and September that large denitrification processes are involved in the removal of NO_y from the southern hemisphere polar vortex. Denitrification occurs during the southern hemisphere winter below ~20 hPa, involving heterogeneous chemistry on PSC particles. Finally, some months exhibit large NO_y^* VMRs near the stratopause during autumn/winter. This results both from year-to-year variation in production of NO_x by EPP and from variation in descent of this NO_x to the middle stratosphere [*Randall et al.*, 2007, 2009].

[41] Figure 10 shows the 1 standard deviation (given in percent) of the zonally averaged data, which is calculated from equations (12)–(14). Much of the middle stratosphere has a 1-sigma value of less than 10%, especially around the tropics. However, at the higher latitudes, during winter/spring months, larger 1-sigma values of ~20–30% are exhibited. This is probably due to strong mixing of NO_y-rich lower stratospheric air with NO_y-depleted air, which descends from the upper stratosphere. Most latitudes in the upper stratosphere/lower mesosphere exhibit variations of larger than 20%, while in the winter polar stratopause region, 1-sigma values are typically greater than 40%. This is a consequence of NO_x-rich air descending from the upper mesosphere, produced largely from EPP activity, although there is a degree of natural variation as EPP alone does not repeat on an annual basis. There appears to be little evidence for a strong seasonal variation apart from at the southern polar vortex where denitrification takes place, yielding 1-sigma values typically greater than 40%.

5.3. Three Month NO_y^* Climatologies

[42] Figure 11 exhibits the four 3 month climatologies: DJF, MAM, JJA, and SON. As these 3 month fields are a combination of monthly data, a more complete geographical representation can be achieved. Here, many of the features discussed in section 5.1 can be clearly seen in the seasonal fields, for example, denitrification in the southern polar winter vortex and EPP at the winter polar stratopause. Due to the SCISAT-1 satellite's repeating annual orbit, only certain latitudes will be sampled for any given month. Consequently, a given bin may have data from only 1 month, while another adjacent bin may have data from 2 or 3 months. This can produce sharp gradients at a given latitude. An example of this can be seen during SON at 70°S where the VMRs changes suddenly from 12 to 16 ppbv (north of 70°S) to

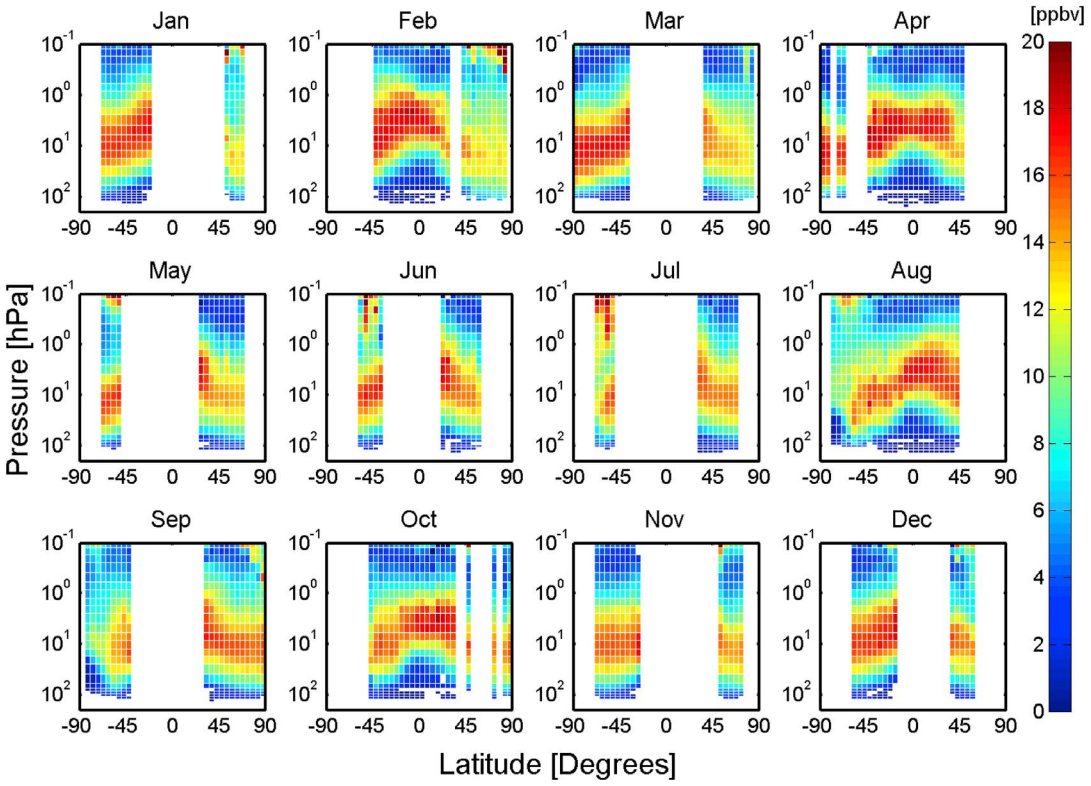

Figure 9. ACE-FTS NO_y^* monthly climatologies for January through December. Values are given in ppbv.

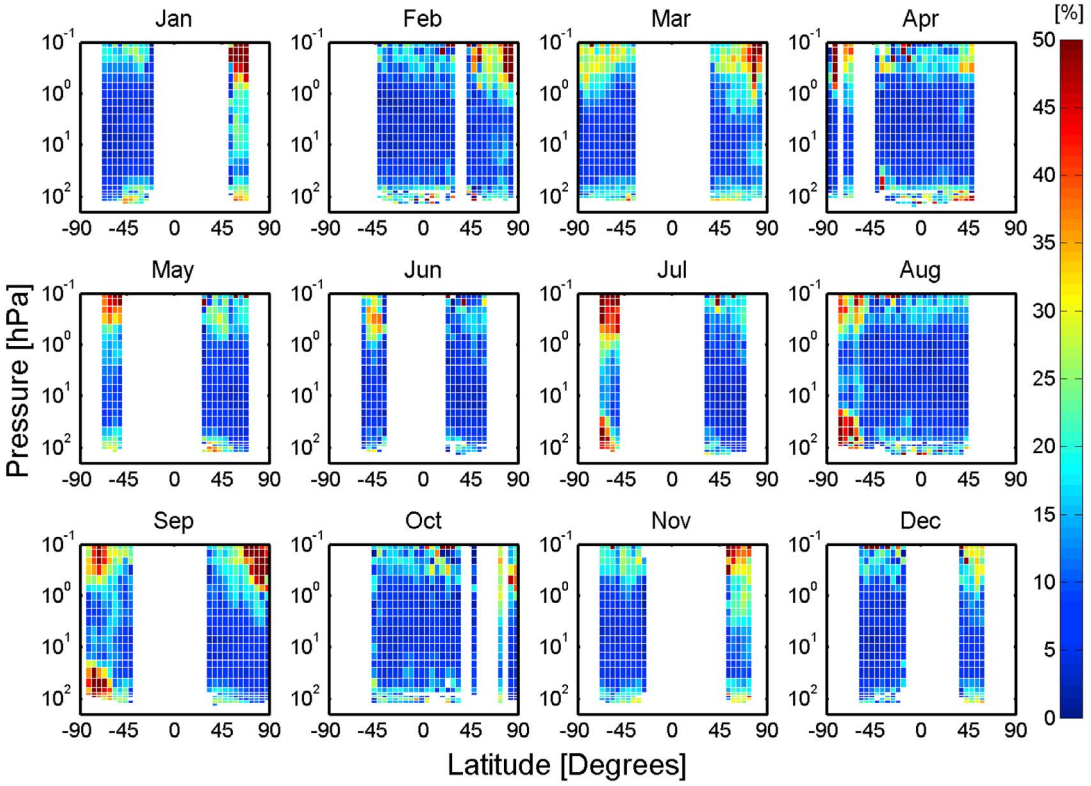

Figure 10. One standard deviation values calculated from the NO_y^* monthly climatological fields. Values are given in percent.

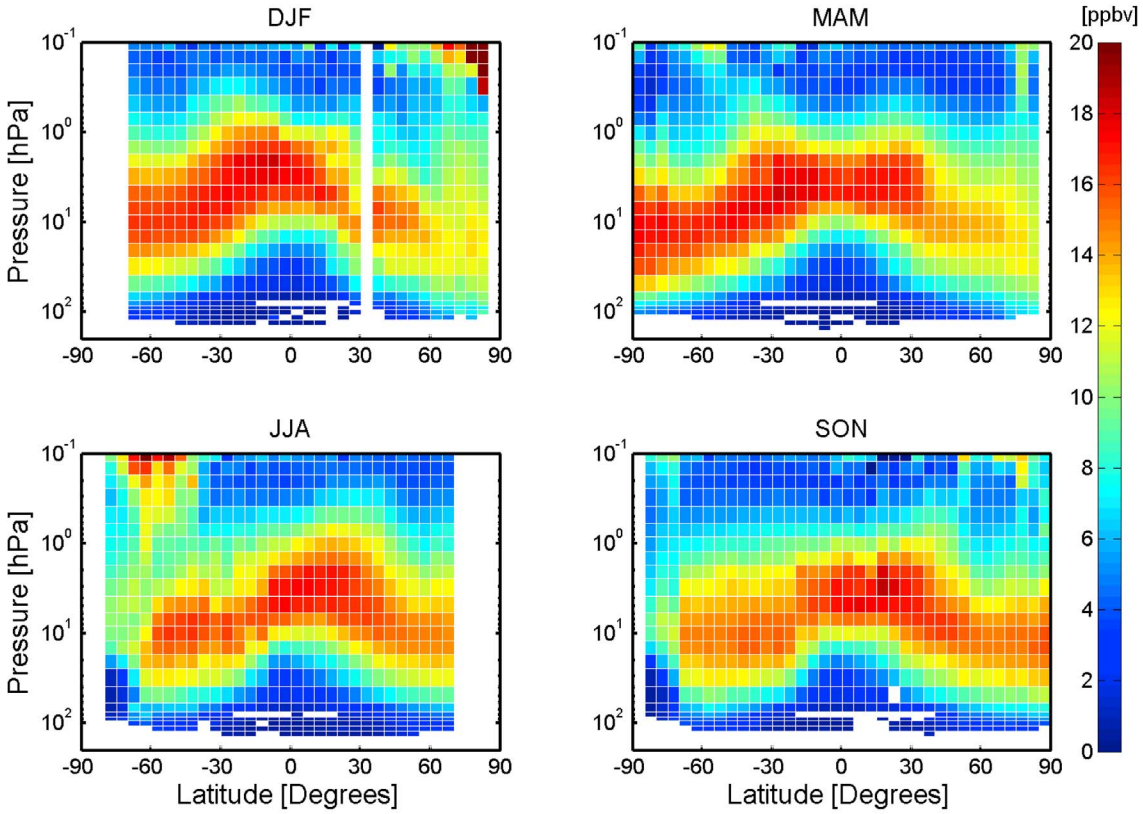

Figure 11. Three month NO_y^* climatological fields: December–January–February (DJF), March–April–May (MAM), June–July–August (JJA), September–October–November (SON). Values are given in ppbv.

6–10 ppbv (90°S–60°S). By examination of Figure 9 it can be seen that south of 70°S, data is only contributed from the month of September, while for 50°S–70°S, data comes from September and November. It is thus advised that for any comparison to these NO_y^* seasonal climatologies, the individual monthly fields be first checked to ascertain the monthly coverage. This information can be found in the suite of data provided in the NO_y^* data products.

6. Discussion

[43] In this section, we validate the NO_y^* climatologies by making comparisons to Odin + photochemical box model NO_y climatology produced by *Brohede et al.* [2008] and to ATMOS data.

6.1. Comparison With Odin and a Photochemical Box Model

[44] First, we compare the ACE-FTS monthly NO_y^* climatologies with the NO_y climatological data set produced by *Brohede et al.* [2008]. This data set comprises Odin OSIRIS NO_2 and Odin SMR HNO_3 combined with synthesized NO, NO_2, 2 × N_2O_5, $ClONO_2$, and HNO_3 mixing ratios using a photochemical box model for January 2002 to December 2006. This provides almost two years of temporal overlap between the Odin and ACE data. The geographical coverage is also good for certain months. The Odin NO_y climatology is produced on a similar latitude grid: 5° degree latitude bands from 85°S to 85°N and altitudes typically from 20 to 40 km at high latitudes and 22–42 km toward the tropics.

[45] Figures 12 and 13 show comparisons for February and September, respectively. These two representative months are chosen as they have similar spatial coverage, thus allowing for a better comparison. However, the systematic differences for all other months are of similar magnitudes and are not shown here. Figures 12a, 12b, 13a, and 13b compare Odin and ACE-FTS NO_y^* climatologies. It can be seen that where there is exact geographical coverage there is good agreement with respect to structure as well as similar peak mixing ratio magnitudes. In Figure 13, both ACE-FTS and Odin show evidence of denitrification in the southern hemisphere polar vortex. However, there is more denitrification in the ACE measurements compared to Odin, which may be a consequence of there being no heterogeneous chemistry or PSCs in the box model calculations. Figures 12c and 13c and Figures 12d and 13d show the absolute (ACE - Odin) and relative difference ((ACE - Odin) / ACE), respectively. We have interpolated the Odin data to the ACE-FTS pressure surfaces. We see that the absolute differences are typically better than 2 ppbv, which in terms of relative difference is better than 20%.

6.2. Comparison With ATMOS NO_y Data

[46] ATMOS was the first space-based instrument to measure NO_y species using solar occultation. It used a Fourier transform spectrometer to observe solar absorption between 600 and 4800 cm^{-1}, with a spectral resolution of 0.01 cm^{-1}

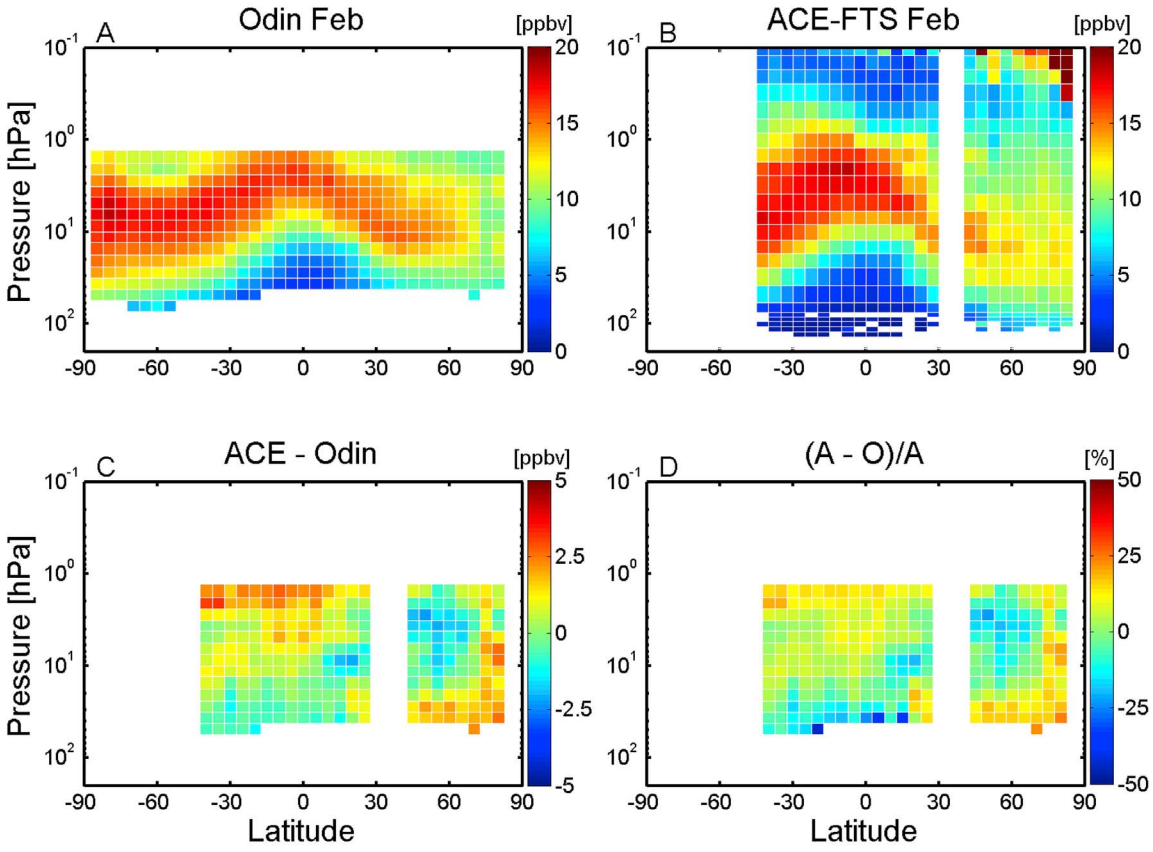

Figure 12. Comparison of the (a) Odin + box model NO_y and (b) ACE-FTS NO_y^* climatologies for the month of February. Also shown are the (c) absolute deviations given in ppbv and (d) relative differences ((ACE-Odin)/ACE), given in percent.

[*Gunson et al.*, 1996]. The ATMOS NO_y climatology was compiled by adding atmospheric measurements of NO, NO_2, HNO_3, $ClONO_2$, and N_2O_5 from four satellite missions spanning 11 years (1985, 1992, 1993, and 1994) [*Irion et al.*, 2002]. Here we compare ACE-FTS NO_y^* to ATMOS NO_y version 3.0 profiles. Due to the estimated 2.6% per decade increase in N_2O [*Forster et al.*, 2007], then over last 15 plus years, it could be reasonable to expect differences of up to 3–6% between the ATMOS and ACE-FTS climatologies. A similar comparison was carried out by *Brohede et al.* [2008], which showed a good level of consistency with the ATMOS climatology. Due to the limited ACE and ATMOS orbital coverage, we find only a few overlapping latitudes between missions. Here, we create a mean ATMOS NO_y profile calculated over 60°S–70°S (November), 40°S–50°S (March), and 15°N–35°N (April). Similarly, we calculate the mean ACE-FTS NO_y^* and Odin + box model (for reference) NO_y profiles combining the representative zonally averaged binned data for the three separate month-latitude bins. It should be noted that we interpolate the ATMOS and Odin data to the same pressure grid as used for ACE-FTS.

[47] Figure 14 presents the ACE-FTS, ATMOS, and Odin + box model climatological profiles for the three separate cases. The vertical dashed lines are the 1 standard deviations calculated from the spread of the measurements at each altitude. The agreement between the three instruments for each individual case shown is very good, where binned profiles show similar vertical features. Pronounced differences are seen in the 60°S–70°S bin at the lowest altitudes, where ACE-FTS is lower than ATMOS by ~3 ppbv close to 80 hPa, while the ATMOS profile shows some oscillating behavior around this altitude. Additionally, above 8 hPa in the 15°N–35°N bin, ACE-FTS is 5 ppbv lower than ATMOS. This former result could possibly be due to the presence of the winter polar vortex, which although it typically breaks up during the latter part of November, may have left a signature in the ATMOS data, as the individual yearly November ATMOS measurements are typically made no later than November 12. Further analysis would be needed in order to separate profiles that are considered to be inside and outside of the vortex. The 1-sigma values for ATMOS and ACE-FTS are of similar magnitudes (generally <2.5 ppbv) for most altitudes. Odin variability is of a larger magnitude (~4 ppbv) at most altitudes outside the tropics, and largest in the tropics where 1-sigma values are >5 ppbv. Overall, the absolute differences between overlapping data sets are generally within the 1-sigma variability of each data set, hence the differences here can be considered statistically insignificant. We also considered the contribution from the scaled initial guess values to these differences. For the 60°S–70°S bin, the observed difference cannot be attributed to using scaled initial guess values since the ACE-FTS NO_y^* at these altitudes is constructed entirely from measurements. The use of these scaled initial guess values could contribute to some

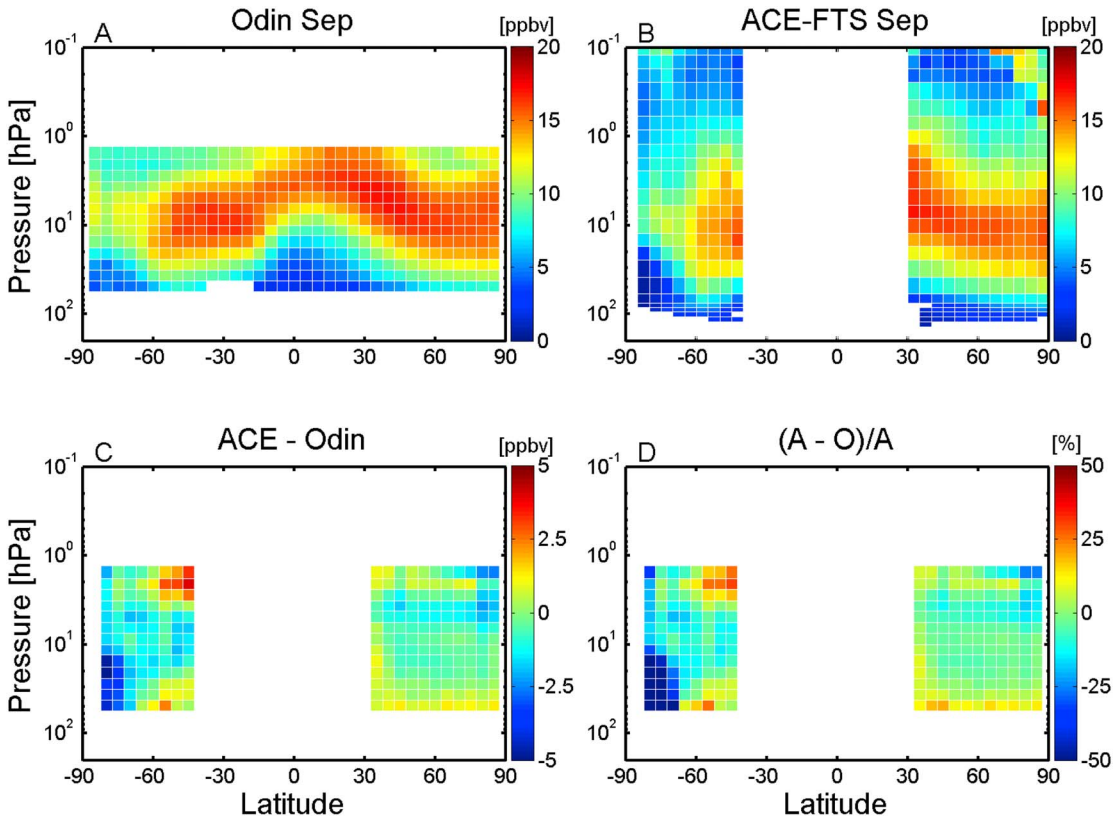

Figure 13. Same as Figure 12 but for the month of September.

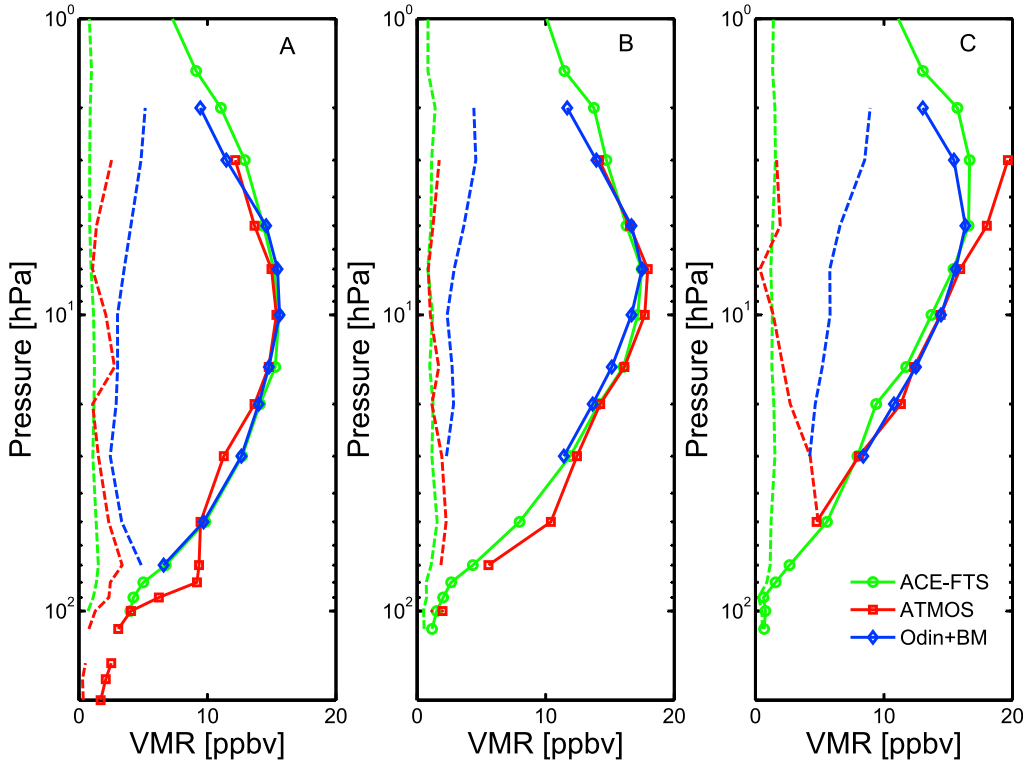

Figure 14. Comparison of mean ACE-FTS, ATMOS, and Odin + box model NO_y climatology profiles for three latitude bins: (a) 60°S–70°S (November), (b) 40°S–50°S (March), and (c) 15°N–35°N (April). Dashed lines indicate the 1-sigma spread of the individual measurements from each instrument at each altitude.

of the difference found in the 15°N–35°N bin. However, these contribute less than 10–15% of the NO_y^* at these pressure levels.

7. Conclusion

[48] We have calculated a NO_y^* zonal average climatology data product using version 2.2 data (plus updates for N_2O_5) from the ACE-FTS instrument. Vertical profiles of six atmospheric nitrogen species were used: NO, NO_2, HNO_3, $ClONO_2$, $2 \times N_2O_5$, and HNO_4. The first five of these species were validated products and are five of the 14 baseline species observed by ACE-FTS, while HNO_4 is a research product only. Measurements included in this NO_y^* product run from February 2004 until February 2009. Individual measurements were first binned into 5° latitude bands, while also separated into 33 pressure bins. Binned data are then subjected to a three-MAD statistical filtering in order to remove measurements that are considered unrepresentative of the most probable state of the atmosphere for a given latitude band and altitude (i.e., outliers). Quality-controlled zonal means are produced, where each contributing measurement was weighted by the inverse of its corresponding fitting uncertainty value.

[49] ACE-FTS NO_y^* climatological peak VMRs typically range between 15 and 20 ppbv and are situated around 10 hPa in the midlatitudes, while are slightly higher in the tropics, at approximately 3 hPa. Strong denitrification is seen during the southern hemisphere winter season at polar latitudes as a result of the strong polar winter jet. The resulting cold temperatures inside the vortex enable the formation of PSCs, on which heterogeneous chemistry can take place, ultimately removing gas phase nitrogen from the stratosphere.

[50] Comparison of the ACE-FTS NO_y^* climatological data set has been made to a NO_y proxy derived from the combination of Odin OSIRIS and SMR measurements (2002–2006) of NO_2 and HNO_3 respectively, with synthesized data provided from a photochemical box model. Agreement between the two climatologies shows systematic differences to be typically less than 20% (2 ppbv) for much of the overlapping coverage (temporally and spatially). ACE-FTS NO_y^* values tend to show more denitrification during the southern hemisphere winter in the polar vortex. This is thought to be related to the fact that the photochemical box model used in the Odin climatology does not include heterogeneous chemistry and PSCs, rendering possibly larger NO_y VMRs. Comparison to mean ATMOS NO_y profiles for three different month-latitude bins shows good agreement with the ACE-FTS (typically better than 3 ppbv) average climatological profiles for these bins.

[51] The ACE-FTS NO_y^* climatological data set is freely available via the ACE website: http://www.ace.uwaterloo.ca/.

[52] **Acknowledgments.** This work has been supported by grants from the Canadian Foundation for Climate and Atmospheric Science (CFCAS) and the Canadian Space Agency (CSA). The Atmospheric Chemistry Experiment (ACE), also known as SCISAT-1, is a Canadian-led mission mainly supported by the Canadian Space Agency. Some support was also provided by the UK Natural Environment Research Council (NERC). We would like to thank the Odin team and the European Space Agency (ESA) for the ease of access and use of the Odin data, with special thanks to Samuel Brohede (University of Chalmers, Sweden). Odin is a Swedish-led satellite project, funded jointly by Sweden (SNSB), Canada (CSA), Finland (Tekes), and France (CNES). We would like to thank the ATMOS team for making their data set available for this work.

References

Abrams, M. C., et al. (1996), On the assessment and uncertainty of atmospheric trace gas burden measurements with high resolution infrared solar occultation spectra from space by the ATMOS experiment, *Geophys. Res. Lett.*, *23*(17), 2337–2340, doi:10.1029/96GL01794.

Bernath, P. F., et al. (2005), Atmospheric Chemistry Experiment (ACE): Mission overview, *Geophys. Res. Lett.*, *32*, L15S01, doi:10.1029/2005GL022386.

Bingham, G. E., D. K. Zhou, B. Y. Bartschi, G. P. Anderson, D. R. Smith, J. H. Chetwynd, and R. M. Nadile (1997), Cryogenic Infrared Radiance Instrumentation for Shuttle (CIRRIS 1A) Earth limb spectral measurements, calibration, and atmospheric O_3, HNO_3, CFC-12, and CFC-11 profile retrieval, *J. Geophys. Res.*, *102*, 3547–3558, doi:10.1029/96JD03508.

Bollinger, M. J., R. E. Sievers, D. W. Fahey, and F. C. Fehsenfeld (1983), Conversion of nitrogen dioxide, nitric acid, and n-propyl nitrate to nitric oxide by gold-catalyzed reduction with carbon monoxide, *Anal. Chem.*, *55*, 1980–1986, doi:10.1021/ac00262a034.

Boone, C. D., R. Nassar, K. A. Walker, Y. J. Rochon, S. D. McLeod, C. P. Rinsland, and P. F. Bernath (2005), Retrievals for the atmospheric chemistry experiment Fourier-transform spectrometer, *Appl. Opt.*, *44*, 7218–7231, doi:10.1364/AO.44.007218.

Bovensmann, H., J. P. Burrows, M. Buchwitz, J. Frerick, S. Noël, V. V. Rozanov, K. V. Chance, and A. P. H. Goede (1999), SCIAMACHY: Mission objectives and measurement modes, *J. Atmos. Sci.*, *56*, 127–150, doi:10.1175/1520-0469(1999)056<0127:SMOAMM>2.0.CO;2.

Bracher, A., et al. (2005), Cross comparisons of O_3 and NO_2 measured by the atmospheric ENVISAT instruments GOMOS, MIPAS, and SCIAMACHY, *Adv. Space Res.*, *36*, 855–867, doi:10.1016/j.asr.2005.04.005.

Brasseur, G., and E. Remsberg (1999), Summary of the MMII intercomparisons for chemistry, in *Models and Measurements Intercomparison II*, edited by J. H. Park et al., *NASA Tech. Memo.*, *NASA TM-1999-209554*, 190–306.

Brohede, S. M., et al. (2007), Validation of Odin/OSIRIS stratospheric NO_2 profiles, *J. Geophys. Res.*, *112*, D07310, doi:10.1029/2006JD007586.

Brohede, S., C. A. McLinden, J. Urban, C. S. Haley, A. I. Jonsson, and D. Murtagh (2008), Odin stratospheric proxy NO_y measurements and climatology, *Atmos. Chem. Phys.*, *8*, 5731–5754, doi:10.5194/acp-8-5731-2008.

Brühl, C., B. Steil, G. Stiller, B. Funke, and P. Jöckel (2007), Nitrogen compounds and ozone in the stratosphere: Comparison of MIPAS satellite data with the chemistry climate model ECHAM5/MESSy1, *Atmos. Chem. Phys.*, *7*, 5585–5598, doi:10.5194/acp-7-5585-2007.

Burrows, J. P., et al. (1999), The Global Ozone Monitoring Experiment (GOME): Mission concept and first scientific results, *J. Atmos. Sci.*, *56*, 151–175, doi:10.1175/1520-0469(1999)056<0151:TGOMEG>2.0.CO;2.

Callies, J., et al. (2004), GOME-2 ozone instrument onboard the European METOP satellites, *Proc. SPIE Int. Soc. Opt. Eng.*, *5549*, 60–70, doi:10.1117/12.557860.

Chance, K., W. A. Traub, D. G. Johnson, K. W. Jucks, P. Ciarpallini, R. A. Stachnik, R. J. Salawitch, and H. A. Michelsen (1996), Simultaneous measurements of stratospheric HO_x, NO_x, and Cl_x: Comparison with a photochemical model, *J. Geophys. Res.*, *101*(D4), 9031–9043, doi:10.1029/96JD00064.

Chu, W. P., and M. P. McCormick (1979), Inversion of stratospheric aerosol and gaseous constituents from spacecraft solar extinction data in the 0.38–1.0 μm wavelength region, *Appl. Opt.*, *18*, 1404–1413, doi:10.1364/AO.18.001404.

Chu, W. P., and M. P. McCormick (1986), SAGE observations of stratospheric nitrogen dioxide, *J. Geophys. Res.*, *91*(D5), 5465–5476, doi:10.1029/JD091iD05p05465.

Crutzen, P. (1971), Ozone production rates in an oxygen-hydrogen-nitrogen oxide atmosphere, *J. Geophys. Res.*, *76*(30), 7311–7327, doi:10.1029/JC076i030p07311.

Cunnold, D. M., et al. (1991), Validation of SAGE II NO_2 measurements, *J. Geophys. Res.*, *96*(D7), 12,913–12,925, doi:10.1029/91JD01344.

Danilin, M. Y. I., M. Koike, G. K. Yue, N. B. Jones, and P. V. Johnston (1999), Nitrogen species in the post-Pinatubo stratosphere: Model analysis utilizing UARS measurements, *J. Geophys. Res.*, *104*(D7), 8247–8262, doi:10.1029/1999JD900024.

Dibb, J. E., E. Scheuer, M. Avery, J. Plant, and G. Sachse (2006), In situ evidence for renitrification in the Arctic lower stratosphere during the

polar aura validation experiment (PAVE), *Geophys. Res. Lett.*, *33*, L12815, doi:10.1029/2006GL026243.

Drummond, J. R., J. T. Houghton, G. D. Peskett, C. D. Rodgers, M. J. Wale, J. Whitney, and E. J. Williamson (1980), The stratospheric and mesospheric sounder on Nimbus 7, *Philos. Trans. R. Soc., Ser. A*, *296*, 219–241, doi:10.1098/rsta.1980.0166.

Evans, W. F. J., J. B. Kerr, C. T. McElroy, R. S. O'Brien, B. A. Ridley, and D. I. Wardle (1977), The odd nitrogen mixing ratio in the stratosphere, *Geophys. Res. Lett.*, *4*(6), 235–238, doi:10.1029/GL004i006p00235.

Eyring, V., et al. (2010), SPARC CCMVal, SPARC report on the evaluation of chemistry-climate models, *SPARC Rep. 5*, World Meteorol. Org., Geneva, Switzerland.

Fahey, D. W., C. S. Eubank, G. Hübler, and F. C. Fehsenfeld (1985), Evaluation of a catalytic reduction technique for the measurement of total reactive odd-nitrogen NO_y in the atmosphere, *J. Atmos. Chem.*, *3*(4), 435–468, doi:10.1007/BF00053871.

Fahey, D., D. Murphy, K. Kelly, M. Ko, M. Proffitt, C. Eubank, G. Ferry, M. Loewenstein, and K. Chan (1989), Measurements of nitric oxide and total reactive nitrogen in the Antarctic stratosphere: Observations and chemical implications, *J. Geophys. Res.*, *94*(D14), 16,665–16,681, doi:10.1029/JD094iD14p16665.

Fahey, D. W., K. K. Kelly, S. R. Kawa, A. F. Tuck, M. Loewenstein, K. R. Chan, and L. E. Heidt (1990), Observations of denitrification and dehydration in the winter polar stratospheres, *Nature*, *344*, 321–324, doi:10.1038/344321a0.

Fischer, H., and H. Oelhaf (1996), Remote sensing of vertical profiles of atmospheric trace constituents with MIPAS limb-emission spectrometers, *Appl. Opt.*, *35*, 2787–2796, doi:10.1364/AO.35.002787.

Fischer, H., et al. (2008), MIPAS: An instrument for atmospheric and climate research, *Atmos. Chem. Phys.*, *8*, 2151–2188, doi:10.5194/acp-8-2151-2008.

Forster, P., et al. (2007), Changes in atmospheric constituents and in radiative forcing, in *Climate Change, 2007: The Physical Scientific Basis, Contribution of Working Group I to the Fourth Assessment Report of the Intergovernmental Panel on Climate Change*, edited by S. Solomon et al., pp. 129–234, Cambridge Univ. Press, Cambridge, U. K.

Funke, B., M. López-Puertas, S. Gil-López, T. von Clarmann, G. P. Stiller, H. Fischer, and S. Kellmann (2005a), Downward transport of upper atmospheric NO_x into the polar stratosphere and lower mesosphere during the Antarctic 2003 and Arctic 2002/2003 winters, *J. Geophys. Res.*, *110*, D24308, doi:10.1029/2005JD006463.

Funke, B., et al. (2005b), Retrieval of stratospheric NO_x from 5.3 and 6.2 μm nonlocal thermodynamic equilibrium emissions measured by Michelson Interferometer for Passive Atmospheric Sounding (MIPAS) on Envisat, *J. Geophys. Res.*, *110*, D09302, doi:10.1029/2004JD005225.

Funke, B., M. García-Comas, M. López-Puertas, N. Glatthor, G. P. Stiller, T. von Clarmann, K. Semeniuk, and J. C. McConnell (2008a), Enhancement of N_2O during the October-November 2003 solar proton events, *Atmos. Chem. Phys.*, *8*, 3805–3815, doi:10.5194/acp-8-3805-2008.

Funke, B., M. López-Puertas, M. Garcia-Comas, G. P. Stiller, T. von Clarmann, and N. Glatthor (2008b), Mesospheric N_2O enhancements as observed by MIPAS on Envisat during the polar winters in 2002–2004, *Atmos. Chem. Phys.*, *8*, 5787–5800, doi:10.5194/acp-8-5787-2008.

Gauss, M., I. S. A. Isakse, D. S. Lee, and O. A. Søvde (2006), Impact of aircraft NO_x emissions on the atmosphere—Tradeoffs to reduce the impact, *Atmos. Chem. Phys.*, *6*, 1529–1548, doi:10.5194/acp-6-1529-2006.

Gille, J. C., and J. M. Russell (1984), The Limb Infrared Monitor of the Stratosphere: Experiment description, performance, and results, *J. Geophys. Res.*, *89*(D4), 5125–5140, doi:10.1029/JD089iD04p05125.

Gille, J. C., P. L. Bailey, and J. M. Russell III (1980), Temperature and composition measurements from the LRIR and LIMS experiments on Nimbus 6 and 7, *Philos. Trans. R. Soc., Ser. A*, *296*, 205–218, doi:10.1098/rsta.1980.0165.

Gille, J. C., J. M. Russell III, P. L. Bailey, H. Fischer, B. W. Gandrud, A. Girard, W. Evans, J. E. Harries, and S. A. Beck (1984), Accuracy and precision of the nitric acid concentrations determined by the Limb Infrared Monitor of the Stratosphere (LIMS) experiment on Nimbus 7, *J. Geophys. Res.*, *89*(D4), 5179–5190, doi:10.1029/JD089iD04p05179.

Gille, J. C., et al. (2008), The High Resolution Dynamics Limb Sounder (HIRDLS) experiment overview, results and temperature validation, *J. Geophys. Res.*, *113*, D16S43, doi:10.1029/2007JD008824.

Glaccum, W., et al. (1996), The Polar Ozone and Aerosol Measurement instrument, *J. Geophys. Res.*, *101*(D9), 14,479–14,487, doi:10.1029/96JD00576.

Grewe, V., M. Dameris, C. Fichter, and R. Sausen (2002a), Impact of aircraft NO_x emissions. Part 1: Interactively coupled climate chemistry simulations and sensitivities to climate-chemistry feedback, lightning and model resolution, *Meteorol. Z.*, *11*(3), 177–186, doi:10.1127/0941-2948/2002/0011-0177.

Grewe, V., M. Dameris, C. Fichter, and D. S. Lee (2002b), Impact of aircraft NO_x emissions. Part 2: Effects of lowering the flight altitude, *Meteorol. Z.*, *11*(3), 197–205, doi:10.1127/0941-2948/2002/0011-0197.

Gunson, M. R., et al. (1996), The Atmospheric Trace Molecule Spectroscopy (ATMOS) experiment: Deployment on the ATLAS Space Shuttle missions, *Geophys. Res. Lett.*, *23*(17), 2333–2336, doi:10.1029/96GL01569.

Höpfner, M., et al. (2007), Validation of MIPAS $ClONO_2$ measurements, *Atmos. Chem. Phys.*, *7*, 257–281, doi:10.5194/acp-7-257-2007.

Intergovernmental Panel on Climate Change/Technology and Economic Assessment Panel (IPCC/TEAP) (2005), *Special Report on Safeguarding the Ozone Layer and the Global Climate System (SROC)*, edited by B. Metz et al., 484 pp., Cambridge Univ. Press, Cambridge, U. K.

Irie, H., et al. (2002), Validation of NO_2 and HNO_3 measurements from the Improved Limb Atmospheric Spectrometer (ILAS) with the version 5.20 retrieval algorithm, *J. Geophys. Res.*, *107*(D24), 8206, doi:10.1029/2001JD001304.

Irie, H., et al. (2006), Validation of stratospheric nitric acid profiles observed by Improved Limb Atmospheric Spectrometer (ILAS)–II, *J. Geophys. Res.*, *111*, D11S03, doi:10.1029/2005JD006115.

Irion, F. W., M. R. Gunson, C. C. Toon, A. Y. Chang, A. Eldering, E. Mahieu, G. L. Manney, and H. A. Michelsen (2002), Atmospheric Trace Molecule Spectroscopy (ATMOS) Experiment Version 3 data retrievals, *Appl. Opt.*, *41*, 6968–6979, doi:10.1364/AO.41.006968.

Jackman, C. H., M. T. DeLand, G. J. Labow, E. L. Fleming, D. K. Weisenstein, M. K. W. Ko, M. Sinnhuber, and J. M. Russel (2005a), Neutral atmospheric influences of the solar proton events in October–November 2003, *J. Geophys. Res.*, *110*, A09S27, doi:10.1029/2004JA010888.

Jackman, C. H., M. T. DeLand, G. J. Labow, E. L. Fleming, D. K. Weisenstein, M. K. W. Ko, M. Sinnhuber, J. Anderson, and J. M. Russell (2005b), The influence of the several very large solar proton events in years 2000–2003 on the neutral middle atmosphere, *Adv. Space Res.*, *35*, 445–450, doi:10.1016/j.asr.2004.09.006.

Kar, J., et al. (2007), Initial comparison of ozone and NO_2 profiles from ACE-MAESTRO with balloon and satellite data, *J. Geophys. Res.*, *112*, D16301, doi:10.1029/2006JD008242.

Kerzenmacher, T., et al. (2008), Validation of NO_2 and NO from the Atmospheric Chemistry Experiment (ACE), *Atmos. Chem. Phys.*, *8*, 5801–5841, doi:10.5194/acp-8-5801-2008.

Kinnison, D. E., et al. (2008), Global observations of HNO_3 from the High Resolution Dynamics Limb Sounder (HIRDLS): First results, *J. Geophys. Res.*, *113*, D16S44, doi:10.1029/2007JD008814.

Kleinböhl, A., H. Bremer, H. Küllmann, J. Kuttippurath, E. V. Browell, T. Canty, R. J. Salawitch, G. C. Toon, and J. Notholt (2005), Denitrification in the Arctic mid-winter 2004/2005 observed by airborne submillimeter radiometry, *Geophys. Res. Lett.*, *32*, L19811, doi:10.1029/2005GL023408.

Koike, M., et al. (2000), Impact of aircraft emissions on reactive nitrogen over the North Atlantic Flight Corridor region, *J. Geophys. Res.*, *105*(D3), 3665–3677, doi:10.1029/1999JD901013.

Kondo, Y., U. Schmidt, T. Sugita, A. Engel, M. Koike, P. Aimedieu, M. R. Gunson, and J. Rodriguez (1996), NO_y correlation with N_2O and CH_4 in the midlatitude stratosphere, *Geophys. Res. Lett.*, *23*(17), 2369–2372, doi:10.1029/96GL00870.

Kumer, J., et al. (1996a), Comparison of correlative data with HNO_3 version 7 from the CLAES instrument deployed on the NASA Upper Atmosphere Research Satellite, *J. Geophys. Res.*, *101*(D6), 9621–9656, doi:10.1029/95JD03759.

Kumer, J., et al. (1996b), Comparison of CLAES preliminary N_2O_5 data with correlative data and a model, *J. Geophys. Res.*, *101*(D6), 9657–9677, doi:10.1029/95JD03767.

Kumer, J. B., S. R. Kawa, A. E. Roche, J. L. Mergenthaler, S. E. Smith, F. W. Taylor, P. S. Connell, and A. R. Douglass (1997), UARS first global N_2O_5 data sets: Application to a stratospheric warming event in January 1992, *J. Geophys. Res.*, *102*(D3), 3575–3582, doi:10.1029/96JD03055.

Kyrölä, E., et al. (2004), GOMOS on Envisat: An overview, *Adv. Space Res.*, *33*, 1020–1028, doi:10.1016/S0273-1177(03)00590-8.

Lee, D. S., I. Köhler, E. Grobler, F. Rohrer, R. Sausen, L. Gallardo-Klenner, J. J. G. Olivier, and F. D. Dentener (1997), Estimations of global NO_x emissions and their uncertainties, *Atmos. Environ.*, *31*, 1735–1749, doi:10.1016/S1352-2310(96)00327-5.

Levelt, P. F., G. H. J. van den Oord, M. R. Dobber, A. Mlkki, H. Visser, J. de Vries, P. Stammes, J. O. V. Lundell, and H. Saari (2006), The Ozone Monitoring Instrument, *IEEE Trans. Geosci. Remote Sens.*, *44*, 1093–1101, doi:10.1109/TGRS.2006.872333.

Liley, J. B., P. V. Johnston, R. L. McKenzie, A. J. Thomas, and I. S. Boyd (2000), Stratospheric NO_2 variations from a long time series at Lauder, New Zealand, *J. Geophys. Res.*, *105*(D9), 11,633–11,640, doi:10.1029/1999JD901157.

Llewellyn, E. J., et al. (2004), The OSIRIS instrument on the Odin spacecraft, *Can. J. Phys.*, *82*, 411–422, doi:10.1139/p04-005.

López-Puertas, M., B. Funke, S. Gil López, T. Von Clarmann, G. P. Stiller, M. Höpfner, S. Kellman, H. Fischer, and C. H. Jackman (2005a), Observation of NO_x enhancement and ozone depletion in the Northern and Southern Hemispheres after the October–November 2003 solar proton events, *J. Geophys. Res.*, *110*, A09S43, doi:10.1029/2005JA011050.

López-Puertas, M., B. Funke, S. Gil López, T. Von Clarmann, G. P. Stiller, M. Höpfner, S. Kellman, G. M. Tsidu, H. Fischer, and C. H. Jackman (2005b), HNO_3, N_2O_5, and $ClONO_2$ enhancements after the October–November 2003 solar proton events, *J. Geophys. Res.*, *110*, A09S44, doi:10.1029/2005JA011051.

Lucke, R. L., et al. (1999), The Polar Ozone and Aerosol Measurement (POAM) III instrument and early validation results, *J. Geophys. Res.*, *104*(D15), 18,785–18,799, doi:10.1029/1999JD900235.

Manney, G., H. Michelson, M. Santee, M. Gunson, F. Irion, A. E. Roche, and N. Livesey (1999), Polar vortex dynamics during spring and fall diagnosed using trace gas observations from the Atmospheric Trace Molecule Spectroscopy instrument, *J. Geophys. Res.*, *104*(D15), 18,841–18,866, doi:10.1029/1999JD900317.

Mauldin, L. E. I., N. H. Zaun, M. P. McCormick, J. H. Guy, and W. R. Vaughn (1985), Stratospheric Aerosol and Gas Experiment II instruments: A functional description, *Opt. Eng.*, *24*, 307–312.

McCormick, M., P. Hamill, T. Pepin, W. Chu, T. Swissler, and L. McMaster (1979), Satellite studies of the stratospheric aerosol, *Bull. Am. Meteorol. Soc.*, *60*, 1038–1046, doi:10.1175/1520-0477(1979)060<1038:SSOTSA>2.0.CO;2.

McElroy, M. B., and J. C. McConnell (1971), Nitrous oxide: A natural source of stratospheric NO, *J. Atmos. Sci.*, *28*, 1095–1098, doi:10.1175/1520-0469(1971)028<1095:NOANSO>2.0.CO;2.

McElroy, C. T., et al. (2007), The Measurement of Aerosol Extinction in the Stratosphere and Troposphere Retrieved by Occultation (MAESTRO) instrument on the SCISAT satellite is a simple, compact spectrophotometer, *Appl. Opt.*, *46*(20), 4341–4356.

McLinden, C. A., S. C. Olsen, B. Hannegan, O. Wild, M. J. Prather, and J. Sundet (2000), Stratospheric ozone in 3-D models: A simple chemistry and the cross-tropopause flux, *J. Geophys. Res.*, *105*(D11), 14,653–14,665, doi:10.1029/2000JD900124.

McLinden, C. A., S. C. Olsen, M. J. Prather, and J. B. Lileyn (2001), Understanding trends in stratospheric NO_y and NO_2, *J. Geophys. Res.*, *106*(D21), 27,787–27,793, doi:10.1029/2000JD000100.

McLinden, C. A., M. J. Prather, and M. S. Johnson (2003), Global modeling of the isotopic analogues of N_2O: Stratospheric distributions, budgets, and the ^{17}O–^{18}O mass-independent anomaly, *J. Geophys. Res.*, *108*(D8), 4233, doi:10.1029/2002JD002560.

Mengistu Tsidu, G., et al. (2004), Stratospheric N_2O_5 in the Austral Spring 2002 as retrieved from limb emission spectra recorded by the Michelson Interferometer for Passive Atmospheric Sounding (MIPAS), *J. Geophys. Res.*, *109*, D18301, doi:10.1029/2004JD004856.

Mengistu Tsidu, G., et al. (2005), NO_y from Michelson Interferometer for Passive Atmospheric Sounding on Environmental Satellite during the Southern Hemisphere polar vortex split in September/October 2002, *J. Geophys. Res.*, *110*, D11301, doi:10.1029/2004JD005322.

Mergenthaler, J. L., et al. (1996), Validation of CLAES $ClONO_2$ measurements, *J. Geophys. Res.*, *101*(D6), 9603–9620, doi:10.1029/96JD00449.

Minschwaner, K., R. Salawitch, and M. McElroy (1993), Absorption of solar radiation by O_2: Implications for O_3 and lifetimes of N_2O, $CFCl_3$, and CF_2Cl_2, *J. Geophys. Res.*, *98*(D6), 10,543–10,561, doi:10.1029/93JD00223.

Montzka, S. A., et al. (2003), Controlled substances and other source gases, in *Scientific Assessment of Ozone Depletion: 2002*, *Global Ozone Res. Monit. Proj. Rep. 47*, chap. 1, pp. 1.1–1.83, World Meteorol. Org., Geneva, Switzerland.

Morgan, C. G., M. Allen, M. C. Liang, R. L. Shia, G. A. Blake, and Y. L. Yung (2004), Isotopic fractionation of nitrous oxide in the stratosphere: Comparison between model and observations, *J. Geophys. Res.*, *109*, D04305, doi:10.1029/2003JD003402.

Mount, G. H., D. W. Rusch, J. M. Zawodny, C. A. Barth, and J. F. Noxon (1984), Measurements of stratospheric NO_2 from the Solar Mesosphere Explorer satellite: 1. An overview of the results, *J. Geophys. Res.*, *89*(D1), 1327–1340, doi:10.1029/JD089iD01p01327.

Murcray, F. J., F. H. Murcray, A. Goldman, D. G. Murcray, and C. P. Rinsland (1987), Infrared Measurements of Several Nitrogen Species Above the South Pole in December 1980 and November–December 1986, *J. Geophys. Res.*, *92*(D11), 13,373–13,376, doi:10.1029/JD092iD11p13373.

Murtagh, D., et al. (2002), An overview of the Odin atmospheric mission, *Can. J. Phys.*, *80*, 309–319, doi:10.1139/p01-157.

Nakajima, H., et al. (2002), Characteristics and performance of the Improved Limb Atmospheric Spectrometer (ILAS) in orbit, *J. Geophys. Res.*, *107*(D24), 8213, doi:10.1029/2001JD001439.

Nakajima, H., et al. (2006), Characteristics and performance of the Improved Limb Atmospheric Spectrometer-II (ILAS-II) on board the ADEOS-II satellite, *J. Geophys. Res.*, *111*, D11S01, doi:10.1029/2005JD006334.

Nevison, C. D., S. Solomon, and R. R. Garcia (1997), Model overestimates of NO_y in the upper stratosphere, *Geophys. Res. Lett.*, *24*(7), 803–806, doi:10.1029/97GL00549.

Newchurch, M. J., et al. (1996), Stratospheric NO and NO_2 abundances from ATMOS solar-occultation measurements, *Geophys. Res. Lett.*, *23*(17), 2373–2376, doi:10.1029/96GL01196.

Offermann, D., K. U. Grossmann, P. Barthol, P. Knieling, M. Riese, and R. Trant (1999), Cryogenic Infrared Spectrometers and Telescopes for the Atmosphere (CRISTA) experiment and middle atmosphere variability, *J. Geophys. Res.*, *104*(D13), 16,311–16,325, doi:10.1029/1998JD100047.

Orsolini, Y. J., G. L. Manney, M. L. Santee, and C. E. Randall (2005), An upper stratospheric layer of enhanced HNO_3 following exceptional solar storms, *Geophys. Res. Lett.*, *32*, L12S01, doi:10.1029/2004GL021588.

Oshchepkov, S., Y. Sasano, T. Yokota, H. Nakajima, N. Uemura, N. Saitoh, T. Sugita, and H. Matsuda (2006), ILAS data processing for stratospheric gas and aerosol retrievals with aerosol physical modeling: Methodology and validation of gas retrievals, *J. Geophys. Res.*, *111*, D02307, doi:10.1029/2005JD006543.

Porter, H. S., C. H. Jackman, and A. E. S. Green (1976), Efficiencies for production of atomic nitrogen and oxygen by relativistic proton impact in air, *J. Chem. Phys.*, *65*, 154–167, doi:10.1063/1.432812.

Randall, C. E., et al. (2002), Validation of POAM III NO_2 measurements, *J. Geophys. Res.*, *107*(D20), 4432, doi:10.1029/2001JD001520.

Randall, C. E., V. L. Harvey, C. S. Singleton, P. F. Bernath, C. D. Boone, and J. U. Kozyra (2006), Enhanced NO_x in 2006 linked to strong upper stratospheric Arctic vortex, *Geophys. Res. Lett.*, *33*, L18811, doi:10.1029/2006GL027160.

Randall, C. E., V. L. Harvey, C. S. Singleton, S. M. Bailey, P. F. Bernath, M. Codrescu, H. Nakajima, and J. M. Russell III (2007), Energetic particle precipitation effects on the Southern Hemisphere stratosphere in 1992–2005, *J. Geophys. Res.*, *112*, D08308, doi:10.1029/2006JD007696.

Randall, C. E., V. L. Harvey, D. E. Siskind, J. France, P. F. Bernath, C. D. Boone, and K. A. Walker (2009), NO_x descent in the Arctic middle atmosphere in early 2009, *Geophys. Res. Lett.*, *36*, L18811, doi:10.1029/2009GL039706.

Ravishankara, A. R., S. J. Daniel, and R. W. Portmann (2009), Nitrous oxide (N_2O): The dominant ozone-depleting substance emitted in the 21st century, *Science*, *326*(5949), 123–125, doi:10.1126/science.1176985.

Reddmann, T., R. Ruhnke, S. Versick, and W. Kouker (2010), Modeling disturbed stratospheric chemistry during solar-induced NO_x enhancements observed with MIPAS/ENVISAT, *J. Geophys. Res.*, *115*, D00I11, doi:10.1029/2009JD012569.

Rees, M. H. (1989), Appendix 5 – Chemical/ionic reactions in the thermosphere, in *Physics and Chemistry of the Upper Atmosphere*, pp. 278–281, Cambridge Univ. Press, New York.

Riese, M., R. Spang, P. Preusse, M. Ern, M. Jarisch, D. Offermann, and K. Grossmann (1999), Cryogenic Infrared Spectrometers and Telescopes for the Atmosphere (CRISTA) data processing and atmospheric temperature and trace gas retrieval, *J. Geophys. Res.*, *104*(D13), 16,349–16,367, doi:10.1029/1998JD100057.

Rinsland, C. P., A. Goldman, D. G. Murcray, F. J. Murcray, and V. M. Devi (1985), Tentative identification of the 780 cm^{-1} ν_4 band Q branch of chlorine nitrate in high-resolution solar absorption spectra of the stratosphere, *J. Geophys. Res.*, *90*(D5), 7931–7943, doi:10.1029/JD090iD05p07931.

Rinsland, C. P., M. R. Gunson, M. C. Abrams, Z. Zander, E. Mahieu, A. Goldman, M. K. W. Ko, J. M. Rodriguez, and N. D. Sze (1994), Profiles of stratospheric chlorine nitrate ($ClONO_2$) from atmospheric trace molecule spectroscopy/ATLAS 1 infrared solar occultation spectra, *J. Geophys. Res.*, *99*(D9), 18,895–18,900, doi:10.1029/94JD01520.

Rinsland, C. P., et al. (1996), ATMOS/ATLAS-3 measurements of stratospheric chlorine and reactive nitrogen partitioning inside and outside the November 1994 Antarctic vortex, *Geophys. Res. Lett.*, *23*(17), 2365–2368, doi:10.1029/96GL01474.

Roche, A. E., J. B. Kumer, J. L. Mergenthaler, G. A. Ely, W. G. Uplinger, J. F. Potter, T. C. James, and L. W. Sterritt (1993), The cryogenic limb array etalon spectrometer (CLAES) on UARS: Experiment description and performance, *J. Geophys. Res.*, *98*(D6), 10,763–10,775, doi:10.1029/93JD00800.

Rozanov, E., L. Callis, M. Schlesinger, F. Yang, N. Andronova, and V. Zubov (2005), Atmospheric response to NO_y source due to energetic electron precipitation, *Geophys. Res. Lett.*, *32*, L14811, doi:10.1029/2005GL023041.

Rusch, D. W., J.-C. Gerard, S. Solomon, P. J. Crutzen, and G. C. Reid (1981), The effect of particle precipitation events on the neutral and ion chemistry of the middle atmosphere: 1. Odd nitrogen, *Planet. Space Sci.*, *29*, 767–774, doi:10.1016/0032-0633(81)90048-9.

Russell, J. M., III, C. B. Farmer, C. P. Rinsland, R. Zander, L. Froidevaux, G. C. Toon, B. Gao, J. Shaw, and M. Gunson (1988), Measurements of odd nitrogen compounds in the stratosphere by the ATMOS experiment on Spacelab 3, *J. Geophys. Res.*, *93*(D2), 1718–1736, doi:10.1029/JD093iD02p01718.

Russell, J. M., III, L. L. Gordley, J. H. Park, S. R. Drayson, W. D. Hesketh, R. J. Cicerone, A. F. Tuck, J. E. Frederick, J. E. Harries, and P. J. Crutzen (1993), The Halogen Occultation Experiment, *J. Geophys. Res.*, *98*(D6), 10,777–10,797, doi:10.1029/93JD00799.

SAGE ATBD Team (2002), SAGE III Algorithm Theoretical Basis Document (ATBD) for transmission level 1b products version 2.1, technical report, NASA Langley Res. Cent., Hampton, Va.

Santee, M., G. Manney, L. Froidevaux, W. Read, and J. Waters (1999), Six years of UARS Microwave Limb Sounder HNO_3 observations: Seasonal, interhemispheric, and interannual variations in the lower stratosphere, *J. Geophys. Res.*, *104*(D7), 8225–8246, doi:10.1029/1998JD100089.

Santee, M. L., G. L. Manney, N. J. Livesey, and W. G. Read (2004), Three-dimensional structure and evolution of stratospheric HNO_3 based on UARS Microwave Limb Sounder measurements, *J. Geophys. Res.*, *109*, D15306, doi:10.1029/2004JD004578.

Santee, M. L., et al. (2007), Validation of the Aura Microwave Limb Sounder HNO_3 measurements, *J. Geophys. Res.*, *112*, D24S40, doi:10.1029/2007JD008721.

Sasano, Y., M. Suzuki, T. Yokota, and H. Kanzawa (1999), Improved Limb Atmospheric Spectrometer (ILAS) for stratospheric ozone layer measurements by solar occultation technique, *Geophys. Res. Lett.*, *26*(2), 197–200, doi:10.1029/1998GL900276.

Schlager, H., P. Konopka, P. Schulte, U. Schumann, H. Ziereis, F. Arnold, M. Klemm, D. Hagen, P. Whitefield, and J. Ovarlez (1997), In situ observations of air traffic emission signatures in the North Atlantic flight corridor, *J. Geophys. Res.*, *102*(D9), 10,739–10,750, doi:10.1029/96JD03748.

Schumann, U. (1997), The impact of nitrogen oxides emissions from the aircraft upon the atmosphere at flight altitudes-results from the AERONOX Project, *Atmos. Environ.*, *31*, 1723–1733, doi:10.1016/S1352-2310(96)00326-3.

Schumann, U., J. Ström, F. Arnold, T. K. Berntsen, P. M. D. F. Forster, J.-F. Gayet, and D. Hauglustaine (2001), Aviation impact on atmospheric composition and climate, in *European Research in the Stratosphere 1996–2000*, edited by G. T. Amanatidis and N. R. P. Harris, chap. 7, pp. 257–307, Eur. Comm., Brussels.

Semeniuk, K., J. C. McConnell, J. J. Jin, J. R. Jarosz, C. D. Boone, and P. F. Bernath (2008), N_2O production by high energy auroral electron precipitation, *J. Geophys. Res.*, *113*, D16302, doi:10.1029/2007JD009690.

Sen, B., G. Toon, G. Osterman, J.-F. Blavier, J. Margitan, R. Salawitch, and G. Yue (1998), Measurements of reactive nitrogen in the stratosphere, *J. Geophys. Res.*, *103*(D3), 3571–3585, doi:10.1029/97JD02468.

Smith, S. E., et al. (1996), Dinitrogen pentoxide measurements from the Improved Stratospheric and Mesospheric Sounder: Validation of preliminary results, *J. Geophys. Res.*, *101*(D6), 9897–9906, doi:10.1029/95JD02465.

Stiller, G. P., G. M. Tsidu, T. von Clarmann, N. Glatthor, M. Höpfner, S. Kellmann, A. Linden, R. Ruhnke, and H. Fischer (2005), An enhanced HNO_3 second maximum in the Antarctic mid-winter upper stratosphere 2003, *J. Geophys. Res.*, *110*, D20303, doi:10.1029/2005JD006011.

Stiller, G. P., et al. (2007), Global distributions of HO_2NO_2 as observed by the Michelson Interferometer for Passive Atmospheric Sounding (MIPAS), *J. Geophys. Res.*, *112*, D09314, doi:10.1029/2006JD007212.

Strong, K., et al. (2005), MANTRA—A balloon mission to study the odd-nitrogen budget of the stratosphere, *Atmos. Ocean*, *43*, 283–299, doi:10.3137/ao.430401.

Strong, K., et al. (2008), Validation of ACE-FTS N_2O Measurements, *Atmos. Chem. Phys.*, *8*, 4759–4786, doi:10.5194/acp-8-4759-2008.

Taylor, F. W., et al. (1993), Remote sensing of the atmospheric structure and composition by pressure modulator radiometry from space: The ISAMS experiment on UARS, *J. Geophys. Res.*, *98*(D6), 10,799–10,814, doi:10.1029/92JD03029.

Thompson, A. M., R. R. Friedl, and H. L. Wesoky (Eds.) (1996), Atmospheric effects of aviation: First report of the subsonic assessment program, *NASA Ref. Publ.*, *1385*, 155–174.

Urban, J., et al. (2005), Odin/SMR limb observations of stratospheric trace gases: Level 2 processing of ClO, N_2O, O_3, and HNO_3, *J. Geophys. Res.*, *110*, D14307, doi:10.1029/2004JD005741.

Vitt, F. M., T. E. Cravens, and C. H. Jackman (2000), A two dimensional model of thermospheric nitric oxide sources and their contributions to the middle atmospheric chemical balance, *J. Atmos. Sol. Terr. Phys.*, *62*, 653–667, doi:10.1016/S1364-6826(00)00049-3.

Volk, C., J. Elkins, D. Fahey, G. Dutton, J. Gilligan, M. Loewenstein, J. Podolske, K. Chan, and M. Gunson (1997), Evaluation of source gas lifetimes from stratospheric observations, *J. Geophys. Res.*, *102*(D21), 25,543–25,564, doi:10.1029/97JD02215.

von Clarmann, T., et al. (2009), Retrieval of temperature, H_2O, O_3, HNO_3, CH_4, N_2O, $ClONO_2$ and ClO from MIPAS reduced resolution nominal mode limb emission measurements, *Atmos. Meas. Tech.*, *2*, 159–175, doi:10.5194/amt-2-159-2009.

Wang, D. Y., et al. (2007a), Validation of MIPAS HNO_3 operational data, *Atmos. Chem. Phys.*, *7*, 4905–4934, doi:10.5194/acp-7-4905-2007.

Wang, D. Y., et al. (2007b), Validation of nitric acid retrieved by the IMK-IAA processor from MIPAS/ENVISAT measurements, *Atmos. Chem. Phys.*, *7*, 721–738, doi:10.5194/acp-7-721-2007.

Waters, J. W., et al. (2006), The Earth Observing System Microwave Limb Sounder (EOS MLS) on the Aura Satellite, *IEEE Trans. Geosci. Remote Sens.*, *44*, 1075–1092, doi:10.1109/TGRS.2006.873771.

Webster, C., R. May, R. Toumi, and J. Pyle (1990), Active nitrogen partitioning and the nighttime formation of N_2O_5 in the stratosphere: Simultaneous in situ measurements of NO, NO_2, HNO_3, O_3, and N_2O using the BLISS diode laser spectrometer, *J. Geophys. Res.*, *95*(D9), 13,851–13,866, doi:10.1029/JD095iD09p13851.

Weinheimer, A. J., J. G. Walega, B. A. Ridley, G. W. Sachse, B. E. Anderson, and J. E. Collins Jr. (1993), Stratospheric NO_y measurements on the NASA DC-8 during AASE II, *Geophys. Res. Lett.*, *20*(22), 2563–2566, doi:10.1029/93GL02627.

Weinheimer, A. J., J. G. Walega, B. A. Ridley, B. L. Gary, D. R. Blake, N. J. Blake, F. S. Rowland, G. W. Sachse, B. E. Anderson, and J. E. Collins (1994), Meridional distributions of NO_x, NO_y, and other species in the lower stratosphere and upper troposphere during AASE II, *Geophys. Res. Lett.*, *21*(23), 2583–2586, doi:10.1029/94GL01897.

Wennberg, P. O., J. G. Anderson, and D. K. Weisenstein (1994), Kinetics of reactions of ground state nitrogen atoms ($^4S_{3/2}$) with NO and NO_2, *J. Geophys. Res.*, *99*(D9), 18,839–18,846, doi:10.1029/94JD01823.

Wetzel, G., et al. (2006), Intercomparison and validation of ILAS-II version 1.4 target parameters with MIPAS-B measurements, *J. Geophys. Res.*, *111*, D11S06, doi:10.1029/2005JD006287.

Wetzel, G., et al. (2007), Validation of MIPAS-ENVISAT NO_2 operational data, *Atmos. Chem. Phys.*, *7*, 3261–3284, doi:10.5194/acp-7-3261-2007.

Wolff, M. A., et al. (2008), Validation of HNO_3, $ClONO_2$ and N_2O_5 from the Atmospheric Chemistry Experiment Fourier Transform Spectrometer (ACE-FTS), *Atmos. Chem. Phys.*, *8*, 3529–3562, doi:10.5194/acp-8-3529-2008.

World Meteorological Organization (WMO) (2003), Scientific assessment of ozone depletion: 2002, *Global Res. and Monit. Proj. Rep. 47*, Geneva, Switzerland.

World Meteorological Organization (WMO) (2007), Scientific assessment of ozone depletion: 2006, *Global Res. and Monit. Proj. Rep. 50*, Geneva, Switzerland.

Yokota, T., H. Nakajima, T. Sugita, H. Tsubaki, Y. Itou, M. Kaji, M. Suzuki, H. Kanzawa, J. H. Park, and Y. Sasano (2002), Improved Limb Atmospheric Spectrometer (ILAS) data retrieval algorithm for Version 5.20 gas profile products, *J. Geophys. Res.*, *107*(D24), 8216, doi:10.1029/2001JD000628.

Zander, R., C. Rinsland, C. Farmer, L. Brown, and R. Norton (1986), Observation of several chlorine nitrate ($ClONO_2$) bands in stratospheric infrared spectra, *Geophys. Res. Lett.*, *13*(8), 757–760, doi:10.1029/GL013i008p00757.

Zander, R., et al. (1996), The 1994 northern midlatitude budget of stratospheric chlorine derived from ATMOS/ATLAS-3 observations, *Geophys. Res. Lett.*, *23*(17), 2357–2360, doi:10.1029/96GL01792.

Ziereis, H., H. Schlager, P. Schulte, P. van Velthoven, and F. Slemr (2000), Distributions of NO, NO_x, and NO_y in the upper troposphere and lower stratosphere between 28° and 61°N during POLINAT 2, *J. Geophys. Res.*, *105*(D3), 3653–3664, doi:10.1029/1999JD900870.

P. F. Bernath, Department of Chemistry, University of York, Heslington, York YO10 5DD, UK.

C. D. Boone, Department of Chemistry, University of Waterloo, 200 University Ave. W, Waterloo, ON N2L 3G1, Canada.

A. Jones, G. Qin, K. Strong, and K. A. Walker, Department of Physics, University of Toronto, 60 St. George St., Toronto, ON M5S 1A7, Canada. (kwalker@atmosp.physics.utoronto.ca)

T. Kerzenmacher, Belgian Institute for Space Aeronomy, Ringlaan-3-Avenue Circulaire, B-1180 Brussels, Belgium.

C. A. McLinden, Environment Canada, 4905 Dufferin St., Toronto, ON M3H 5T4, Canada.

M. Toohey, Leibniz Institute of Marine Sciences at University of Kiel (IFM-GEOMAR), Duesternbrooker Weg 20, D-24105 Kiel, Germany.